frontiers | Frontiers in Earth Science

TYPE Original Research
PUBLISHED 09 January 2023
DOI 10.3389/feart.2022.895530

Check for updates

OPEN ACCESS

EDITED BY
Wenjing Lin,
Chinese Academy of Geological Sciences, China

REVIEWED BY
Wei Shi,
Chinese Academy of Geological Sciences (CAGS), China
Dawen Zhang,
Zaozhuang University, China

*CORRESPONDENCE
Feng Qingda,
fengqingda@mail.cgs.gov.cn
Li Fucheng,
lifucheng@mail.cgs.gov.cn

SPECIALTY SECTION
This article was submitted to Structural Geology and Tectonics, a section of the journal Frontiers in Earth Science

RECEIVED 14 March 2022
ACCEPTED 05 August 2022
PUBLISHED 09 January 2023

CITATION
Yang Z, Qingda F, Fucheng L, Linyou Z, Chao Z, Senqi Z, Dunpeng L, Zhen Y, Jian S, Lei F and Zhaoxuan N (2023), Insights into the late Cenozoic structural deformation and tectonic stress field of the Qiabuqia region, Gonghe Basin, northeastern Qinghai–Tibetan Plateau. *Front. Earth Sci.* 10:895530. doi: 10.3389/feart.2022.895530

COPYRIGHT
© 2023 Yang, Qingda, Fucheng, Linyou, Chao, Senqi, Dunpeng, Zhen, Jian, Lei and Zhaoxuan. This is an open-access article distributed under the terms of the Creative Commons Attribution License (CC BY). The use, distribution or reproduction in other forums is permitted, provided the original author(s) and the copyright owner(s) are credited and that the original publication in this journal is cited, in accordance with accepted academic practice. No use, distribution or reproduction is permitted which does not comply with these terms.

Insights into the late Cenozoic structural deformation and tectonic stress field of the Qiabuqia region, Gonghe Basin, northeastern Qinghai–Tibetan Plateau

Zhang Yang[1], Feng Qingda[1]*, Li Fucheng[1]*, Zhang Linyou[1], Zhang Chao[2], Zhang Senqi[1], Li Dunpeng[3], Yan Zhen[4], Song Jian[1], Fu Lei[1] and Niu Zhaoxuan[1]

[1]Center For Hydrogeology and Environmental Geology Survey, China Geological Survey, Baoding, China, [2]College of Energy, Chengdu University of Technology, Chengdu, China, [3]Zijin Mining College, Fuzhou University, Fuzhou, China, [4]Institute of Geology, Chinese Academy of Geological Sciences, Beijing, China

In addition to overall uplift of the Qiabuqia region during the Late Cenozoic, three deformation stages can be identified in the northeastern Qinghai–Tibet Plateau. Specifically, these deformation stages were recognized in areas east of the Gonghe Basin that surrounds Waliguan Mountain and include: 1) Late Miocene to Late Pliocene deformation—dominated by thrust napping with dextral strike-slipping; 2) Early Pleistocene to late middle period of Pleistocene deformation—fault structures were dominated by the dextral strike-slipping with thrust napping; and 3) end of Late Pleistocene to Middle Holocene deformation—thrust napping slowed down and finally braked, while the shallow surface began to loosen and extend at Qiabuqia region's rear-edge. DR4 borehole drilling data indicate that the Xiangshuihe Formation's buried depth is ~1,000 m. The Xianshuihe Formation's top section is characterized by normal fault–type (NF) tectonic stress, while the maximum principal tectonic stress (σ1) is perpendicular and the minimum principal tectonic stress (σ3) is horizontal. In contrast, the deep basement is characterized by thrust fault (TF) and strike-slip (SS) tectonic stress, while the σ1 is in the NE-SW direction, ranging from 20.1° to 75.3° with an average of 40.0°. Based on the aforementioned observations, it can be inferred that there are three sets of hidden faults in the basement of the Qiabuqia region: 1) the NW–NNW trending compressional–torsional faults; 2) the NE trending tensional–torsional faults; and 3) the NWW trending compressional–torsional faults. The findings in this study can potentially offer a robust geological basis for exploring and utilizing hot, dry rock resources within the Gonghe Basin.

KEYWORDS

thrust nappe, strike-slip fault, normal fault, tectonic stress field, hot dry rock, Late Cenozoic, Gonghe Basin

1 Introduction

The concentration of geostress in the rocks surrounding the borehole wall affects how compression fractures in the borehole walls will open, while the far-field minimum principal geostress direction determines compression fractures' extensional mode. In summary, the hydraulic fractures' extensional direction is generally perpendicular to that of the minimum principal stress (Wu et al., 2014; Zhang et al., 2017; Zeng et al., 2019). Therefore, drilling along the direction of maximum principal stress is beneficial for constructing artificial reservoirs and connecting injection and production wells. In highly heterogeneous reservoirs punctuated by fault structures, hydraulic fracture formation and distribution is governed by both the current geostress field and spontaneous fractures resulting from the paleotectonic stress field. In addition, active faults can indicate the arrangement/direction of hot, dry rock geothermal wells, as they frequently indicate where energy is concentrated, which in turn can be followed to the high-temperature geothermal reservoir (Yang et al., 2017). Consequently, accurately analyzing the deep paleotectonic stress field and deducing the direction and characteristics of hidden fault structures within the basement is a key process in exploring and utilizing hot, dry rock resources.

Extensive compressional and strike-slip structures are dispersed throughout the Gonghe Basin and surrounding orogenic belts; thus, they have received widespread attention (Wang et al., 1988; Yuan et al., 2004a; Jiang et al., 2008; Chang et al., 2009; Craddock, 2011; Craddock et al., 2011; Craddock et al., 2014). In contrast, normal faults that are distributed throughout the basin, and are also characterized by small displacement, are often overlooked. In recent years, seven groups of stepped and horst–graben–shaped normal fault structural assemblages have been identified in the Qiabuqia area of the northeastern Gonghe Basin. Contrarily, thrust nappe and strike-slip structures developed at Waliguan Mountain, east of the Qiabuqia region. As such, both vertical and horizontal structural changes resulting from tectonic stress must be considered to accurately characterize hidden fault structures.

It has been established that geological bodies that affect and record geological structural histories become progressively younger as the targeted underground engineering area is approached. Thus, a direction analysis of stress generated by modern geostress has a higher reliability. To fill the resulting gap, this work focuses on analyzing the brittle tectonic deformation and neotectonic components that cut across the older deformational fabrics, which includes evaluating the folds, faults, and arrangement of quartz or calcite veins based on Triassic geological bodies in the Qinghai South Mountain–Waliguan Mountain area. This study locale was selected because it is close to Qiabuqia town. Moreover, Late Miocene and younger sedimentary strata in the study area were also analyzed to obtain numerous types of structural information. Simultaneously, all non-tectonic influence factors were excluded. The process described before provides a strong foundation for determining the tectonic stress field and deep basement fault structures that have developed since the Late Cenozoic.

In summary, this study combined field geological surveys, fault analysis, remote sensing imagery interpretation, and geochronological analysis to 1) determine the formation sequences of the thrust nappe structures and small displacement normal faults and 2) ascertain study area's tectonic setting and evolutionary history. Next, the results from the Late Cenozoic tectonic deformation analysis were implemented, and the Qiabuqia area's deep tectonic stress field and hidden basement faults were simulated using Anderson's theory of faulting (Anderson, 1951), Riedel shear model (Harding, 1974), and bow-and-arrow rule (Elliott, 1976).

2 Regional geological setting

The Gonghe Basin is located in the northeastern region of the Qinghai–Tibetan Plateau. Tectonically, it is part of Qinghai–Tibet Plateau's extensional front edge, which leads toward the intra-continents (Yuan et al., 2004b). The Gonghe Basin is situated on the central–eastern part of an active crustal block that is surrounded by three giant left-lateral strike-slip faults—the NEE-trending Altyn fault, NWW-trending Qilian Mountain–Haiyuan fault, and approximately EW-trending East Kunlun fault (Yuan et al., 2004b; Li et al., 2010). Since the Late Cenozoic, the Qinghai–Tibetan Plateau's northeastern margin has undergone significant deformation in response to the Indo–Asian plate collision and subsequent orogeny. Thus, the area's folds, thrusts, and strike-slip faults are extensively developed. These structural deformation characteristics indicate that this region is undergoing crustal shortening and strike-slip shearing, as well as the clockwise rotation associated with vertical uplift (Deng et al., 2002; Zhang et al., 2006a).

The Qiabuqia area is located on the Gonghe Basin's northeastern margin, nestled on the southwestern side of the ZongWuLong–Qinghai South Mountain tectonic belt (Figure 1A). The most striking fault structures on the belt's northeastern side include a fault (F2) with anti-S arc bending at northeastern Dongwaliguan, fault (F3) at the ZongWuLong–Qinghai South Mountain's southern margin, and Duolonggou curviplanar fault (F4) (Figure 1B). Most previous studies suggest that these arcuate tectonic belts are 1) a consequence of structural deformation during the Late Cenozoic and 2) correlated with the Qinghai–Tibetan Plateau's uplift and eastward extrusion (Zhang et al., 2006a; Wang et al., 2006; Yin, 2010). Extrusion of these blocks was accommodated by strike-slip activity that occurred within the

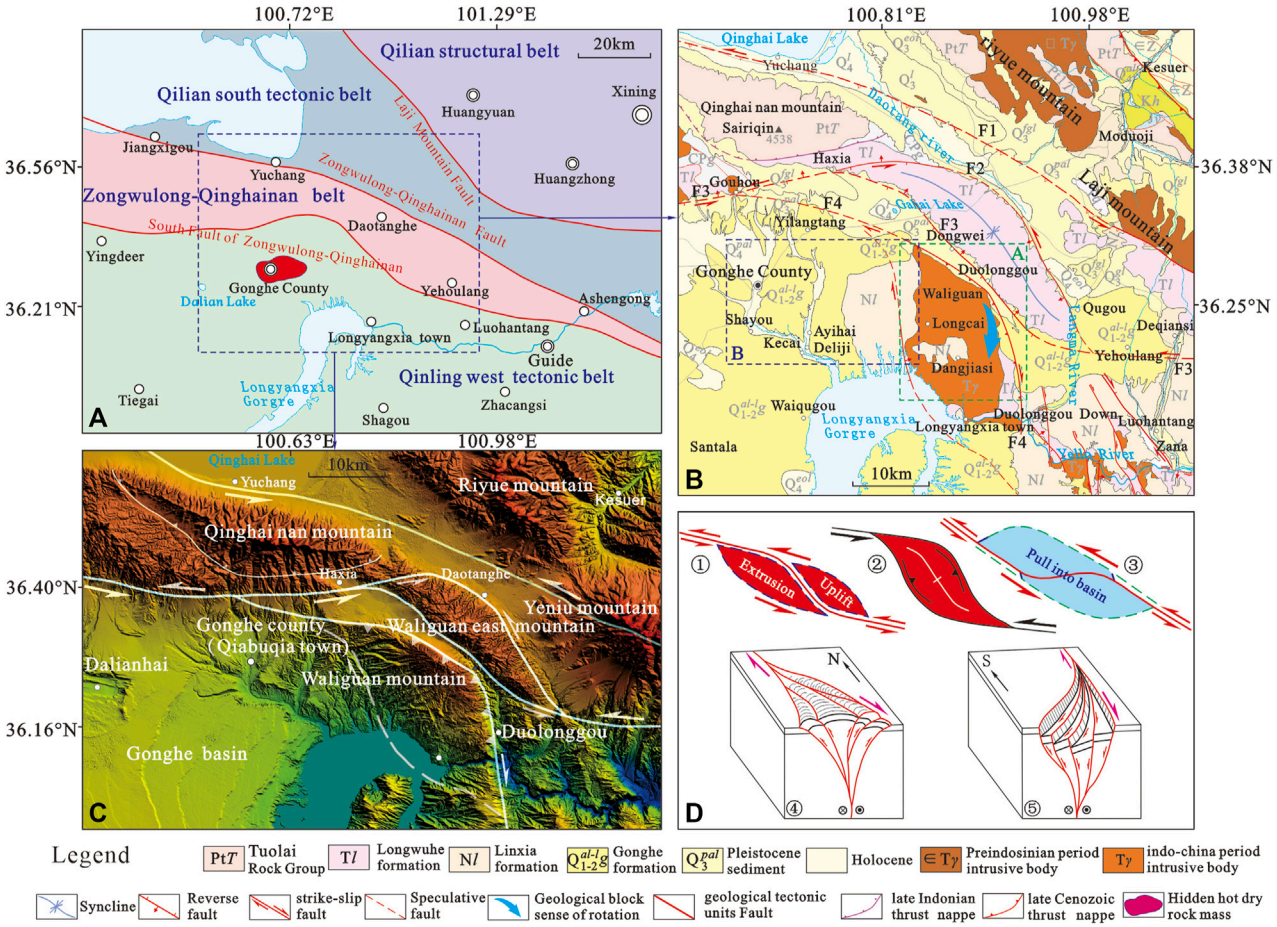

FIGURE 1
(A) Geological map of the Qiabuqia area showing major tectonic unit divisions; **(B)** regional geological map of the Qiabuqia area; **(C)** digital elevation model (DEM) and distribution map depicting main boundary faults; and **(D)** diagram of geomorphological changes caused by strike-slip fault bending (① restricted bending of the left strike-slip fault to form the strike-slip-squeezing uplift at Yeniu Mountain, ② strike-slip-squeezing uplift caused by paired low-curvature restricted bending of the Waliguan and East Waliguan Mountains, ③ fusiform–rhombus composite pull-apart basin formed when the left-lateral strike-slip fault bending stress was released, and ④ + ⑤ horsetail structure at the end of the strike-slip fault: ④ compressional horsetail structure and ⑤ stretching the horsetail structure).

interior of the arcuate tectonic belts and at the marginal faults (Zhang et al., 2004; Zhang et al., 2006b).

The arcual faults mentioned before each behave differently in response to structural location. To accommodate the local contraction, some portions of the arcual faults produced strike-slip–extrusion uplift, resulting in restricted bending, as well as rotation along the vertical axis (Luyendyk et al., 1980; Westaway, 1995; Cowgill et al., 2004). Other parts of the arcual faults were formed when bending stress was released, which produced the strike-slip, pull-apart basin to accommodate extensional bending (Figure 1D) (Crowell and Dickinson, 1974; Christie-Blick and Biddle, 1985). Furthermore, two or more strike-slip faults depicting lip-shaped strikes are referred to as “paired bending” (Mann, 2007)—a feature similar to the arcuate bending fractures seen along Waliguan Mountain and the East Waliguan Mountain boundary (Figure 1C). “Paired bending” commonly occurs in strike-slip systems and probably reflects crustal thickening and uplift at the restricted bending site and volumetric balance between crustal thinning and basin formation at the site where bending stress was released (Woodcock and Fischer, 1986). The tail ends of the strike-slip faults are commonly scattered as horsetail shapes, forming positive and negative flower structures, respectively (Lowell, 1972; Sylvester and Smith, 1976; Harding, 1985; Dooley et al., 1999). Consequently, the strike-slip bending faults were ultimately absorbed and adjusted by oblique and dip-slip faulting (McClay and Bonory, 2001).

Based on regional geological investigation and drilling data, the sedimentary cover in the Qiabuqia area primarily

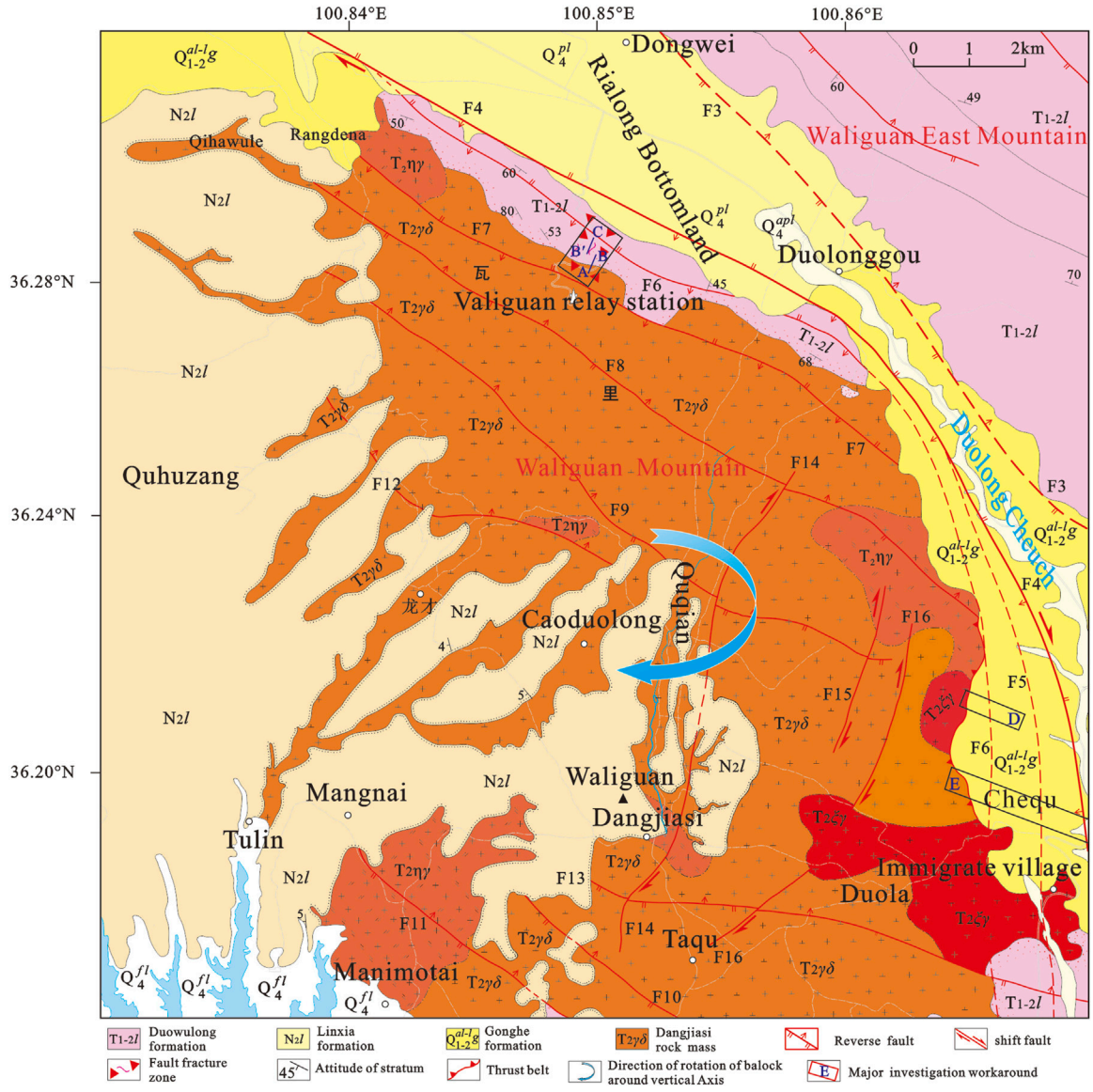

FIGURE 2
Geologic map of the thrust nappe at Waliguan Mountain (Area A in Figure 1B) (Chen et al., 2016).

includes the Miocene Xianshuihe Formation (N1x), Pliocene Linxia Formation (N2l), Early–Middle Pleistocene Gonghe Formation ($Q^{al-l}_{1-2}g$), Middle–Late Pleistocene Yellow River alluvial sand and gravel strata (Q_{2-3}^{al}), and other Quaternary strata (Figure 1B). Emplacement time studies indicate that the Xianshuihe and Linxia formations are 20.8–7.8 Ma and 7.8–2.6 Ma, respectively (Fang et al., 2005; Fang et al., 2007). The top interfaces of both formations show diachroneity. Furthermore, the Gonghe Formation and Yellow River alluvial strata show an emplacement time of 2.24–0.10 Ma (Xu et al., 1984) and 174.5–91.0 ka (Sun et al., 2007), respectively.

3 Geological characteristics of the strike-slip–thrust nappe at Waliguan Mountain

The strike-slip–thrust nappe at Waliguan Mountain is located at the northern part of the Xinjie–Waliguan strike-slip–extrusion uplift zone and constitutes the front part of the Gonghe quasi-thrust nappe (Zhang et al., 2020). Situated ~25 km east of Qiabuqia town, the thrust nappe is a NW–SN–trending arcuate mountain measuring ~12 km in width (east to west) and ~28 km in length (south to north). It mainly consists of Middle Triassic Dangjiasi pluton (T2γδ) and Early–Middle Triassic

LongWuHe Formation. The thrust nappe's geomorphology is described as "tilt-up on the east and being subducted on the west". The thrust nappe's western slope is relatively long and flat, whereas the eastern slope is relatively steep and short. The eastern boundary is defined by the NE-extruding Duolonggou curviplanar fault (F4) (Figure 1B). On the eastern side, the thrust nappe and dextral strike-slip structures overlie the Gonghe Formation and the Middle–Late Pleistocene Yellow River alluvial strata. On the western side, the thrust nappe is unconformably overlain by the Pliocene Linxia Formation (Figure 2).

To the west of Waliguan Mountain, the bottom of the Gonghe Basin's Linxia Formation overlies the western Dangjiasi magmatic body creating an angular unconformity. The boundary is marked by the presence of basal conglomerate–like granitic weathered sands that show poor sorting, low degree of rounding, and *in situ* transportation and accumulation. Apatite fission track (AFT) thermochronological data suggests that the strike-slip–thrust nappe started in the Late Miocene and ended in the Middle–Late Pleistocene period.

3.1 The Duolonggou arc–shaped strike-slip–thrust nappe (F4)

The Duolonggou strike-slip–thrust nappe (F4) serves as the major fault boundary associated with the Waliguan Mountain thrust nappe and forms a NE-extruding arc shape that peaks at Duolonggou Hamlet. This nappe's northwestern section strikes to the NWW, although most of it remains hidden. In the northwestern section, the Gonghe Formation and Middle–Late Pleistocene Old Yellow River alluvial gravel deposit jointly formed an eroded hilly landform, which was superimposed by a diluvial fan during the latter part of the Late Pleistocene–Holocene. All these features indicate that the northwestern section of this arc formed during a relatively earlier time. The southern portion extends in the S-N direction and is a dextral strike-slip and thrust nappe with a west dipping fault plane and a dip angle of 60°–70°. The 0.05- to 1.0-km-wide broken belt is mainly composed of cataclasites and fault gouges. Many branch faults in the southern section of the Duolonggou curviplanar fracture (F4) developed within the Gonghe Formation. The footwall of the local main fault also has very thick deposits of autochthonous granitic weathered sands, indicating that this fault (F4) underwent intense impulse-type thrust napping during the Early–Middle Pleistocene. Consequently, rapid uplift and erosion occurred at Waliguan Mountain. In addition, the fact that the branch faults developed on the west side of the southern Duolonggou arc's main fault and the Middle–Late Pleistocene Yellow River alluvial deposit is the youngest affected stratum suggest that the southern section continued to move until the middle of the Late Pleistocene. The geological features of three structural profiles controlling this fault are described as follows:

(1) Structural profile along the road paralleling Waliguan relay station's eastern foot

This profile was measured along a part of the Waliguan relay station that is located at the artificial excavation slope on the northern side of a highway near the mountain pass. During data collection, point B shifted northward to point B′ due to the impact of the Holocene slope deposits east of the A–B section. The A–B and B′–C sections make up the structural section shown in the A–C area of Figure 2 and comprise a total length of 0.43 km.

The profile was constructed by carrying out all measurements within the intrusive contact line and fault fractural zone of the Dangjiasi rock mass (Figure 3D). While the LongWuHe Formation captures the uneven sizes distributed throughout the Dangjiasi rock mass, it also depicts granitic apophyses and veins, all of which were cut and destroyed by joint cracks and fractured rocks associated with later stage brittle faults (Figures 3B,C,F). In addition, alternating occurrences of strong and weak strain bands in the brittle deformational provinces are also presented in this profile (Figures 3B,C,F). Individual fault bands have a width of 0.1–10 m and are mainly composed of cataclasites, fault gouges, and tectonic lenses. The brick-red color also developed locally due to iron dissemination (Figures 3B,F,G). The dragged tectonic lenses and the hanging and foot walls indicate thrusting to the NE-E, with the fault plane dipping to the SW-W at a 38°–70° angle. Plagiotropous striations superimposed on late-stage joint surfaces illustrate the dextral strike-slip attributes and indicates that there was a substantial SSE-trending horizontal displacement component during the late stage (Figures 3A,E). Due to the presence of Holocene slope washes covering the area, this profile only controls the local part (about 0.43 km) of the Duolonggou arc fault zone's middle region. However, it can be inferred that the entire fault fracture zone is wider than 1.0 km.

(2) Structural profile along the Duolonggou South Mountain's eastern foot.

The second profile was measured along the eastern foot of the Duolonggou South Mountain (Area D in Figure 2). At the profile's western end, the Dangjiasi rock masses thrust westward over the Gonghe Formation. Due to the overlying Holocene slope deposits, no nappe interface outcroppings are visible. The fault plane is believed to dip to the NWW at ~60° (Craddock et al., 2014). The footwall (Gonghe Formation) has been tilted and distorted in response to Waliguan Mountain thrusting. As a consequence, the dip angle has dropped from 20° to 50° in the western portion to 6°–10° a few kilometers to the east.

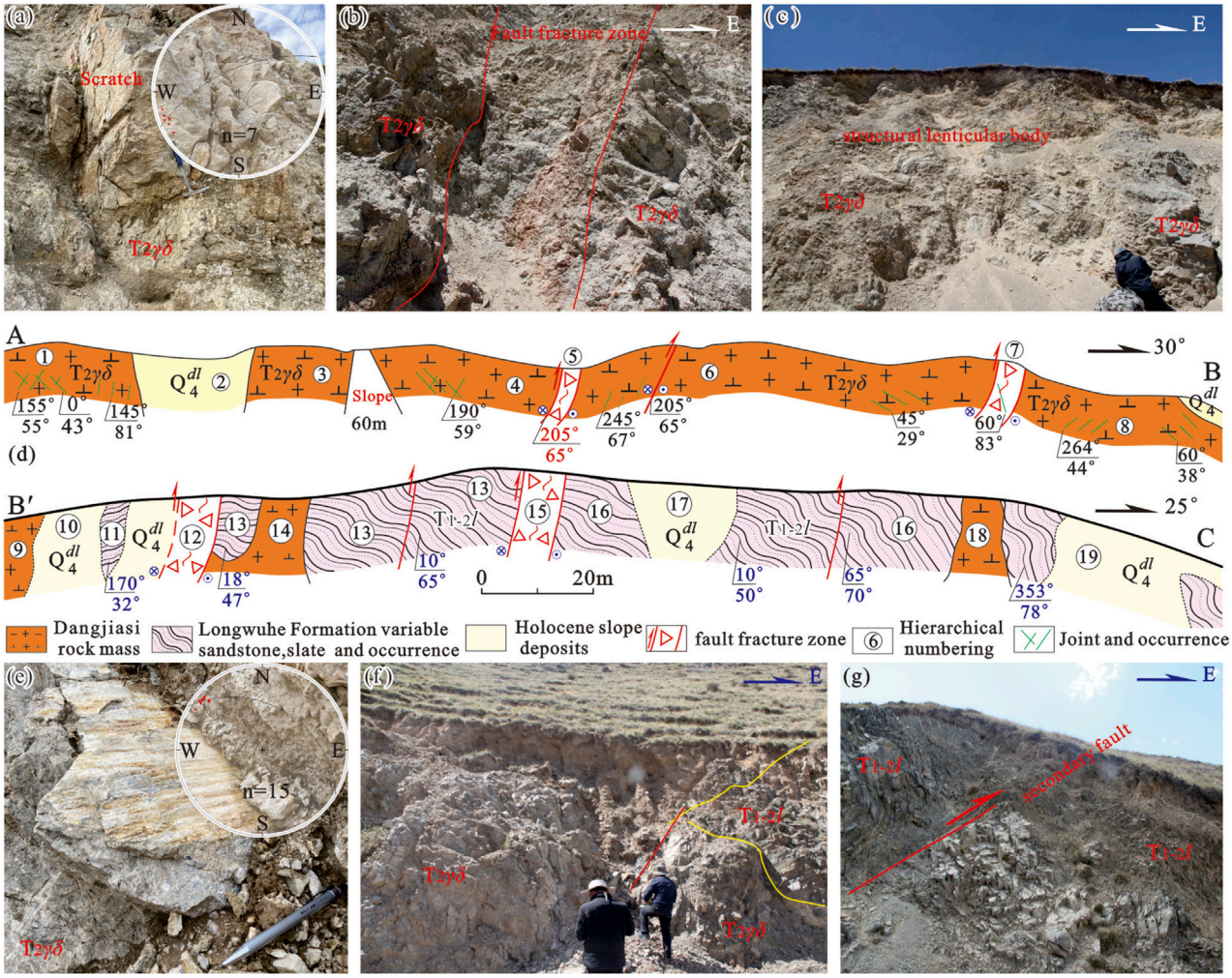

FIGURE 3
Measured structural profile along the road paralleling Waliguan relay station's eastern foot. **(d)** Coordinate of starting point A: E100°53′56″, N36°17′28″; coordinate of end point B: E100°53′56″, N36°17′28″; coordinate of starting point B′: E100°53′65″, N36°17′33″; coordinate of end point C: E100°53′59″, N36°17′40″.

Notably, there's an ~80 m high outcrop at the profile's western segment, where the dip angles of the Gonghe Formation's growth strata gradually reduce from bottom to up. The strata, which dip to the SEE at a 31° angle, are unconformably covered by a stratum that also dips to the SEE but with a dip angle of 22°. Likewise, the eastern segment has fan-inclined Gonghe Formation growth strata that are also unconformably covered by overlying strata (Craddock et al., 2014). This phenomenon suggests that 1) the Duolonggou arc fault may have undergone impulse-type thrust nappe activities during sedimentation of the Gonghe Formation in the Early to Middle Pleistocene and 2) East Waliguan Mountain may have hedged westward, resulting in the Duolonggou ramp valley experiencing compressional stress and the Gonghe Formation undergoing folding deformation.

(3) Structural profile of the Chiqugou

A profile of the main fracture comprising the Duolonggou curviplanar fracture (F4) is visible ~50 m west of the Chiqugou culvert along the Gonghe–Gahaitan–Longyangxia roadway (Region E in Figure 2). In the profile, the Dangjiasi rock mass thrusted onto the Gonghe Formation's Middle–Late Pleistocene Yellow River alluvial deposit at a high angle (Figure 4C). This dextral strike-slip and thrust fault strikes roughly south to north and is characterized by a fault plane dipping to the west at a 60°–70° angle. The fracture zone is 50–100 m wide and is primarily composed of clastic granite and fault breccia. Fault scratches are clearly visible on the K-feldspar located within the hanging wall's granite veins (Figure 4E). Thick layers of granitic weathered sands were deposited on the fault's footwall,

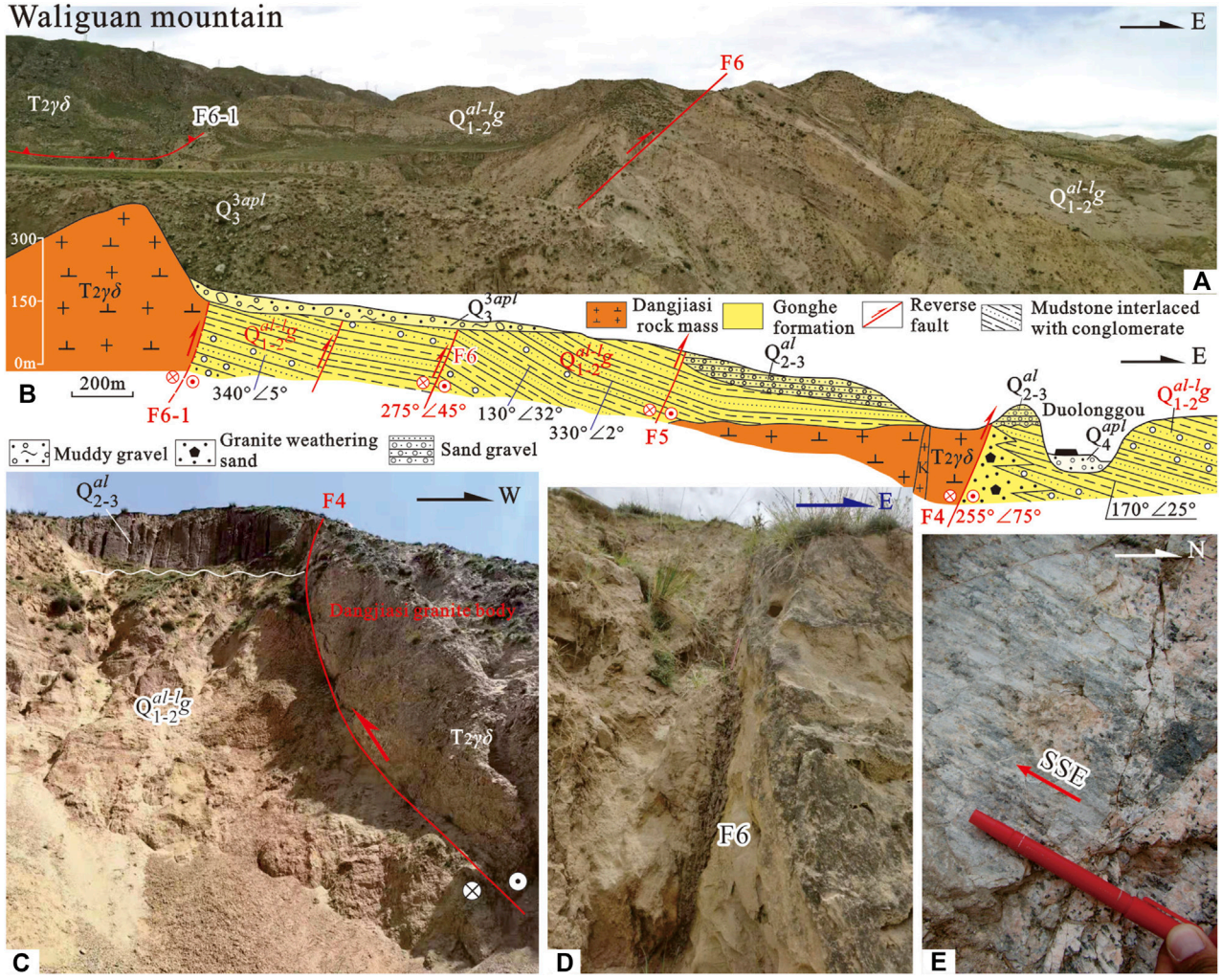

FIGURE 4
(A,B) Photo and profile of the Chiqugou route.

representing syntectonic denudation deposits induced by the hanging wall's strong thrust nappe and structural uplift. The Gonghe Formation has been tilted and distorted due to faulting activity, as evidenced by its attitude of 170°∠25°. Thermoluminescence dating of the low-order fault gouge indicates that the last activity occurred ~110,000 years ago, during the early stage of the Late Pleistocene. This suggests that the major fault in the southern portion was mostly active in the Early–Middle Pleistocene. During the later period, the branch faults continued to move westward.

F4, F5, and a series of secondary faults are all present in the western Gonghe Formation. Thus, grey-yellow, grey-white, grey-green, and grey-black mudstone; argillaceous siltstone mixed with multicolored, medium-coarse grained sandstone; and poorly cemented sandy conglomerates are found along this profile. The F5 fracture zone characteristics cannot be discerned due to collapse and overlying slope deposits, while F6 depicts a fault plane attitude of 275°∠45° and a 0.04–0.10 m wide fault fracture zone (Figures 4A,D). The bottom portion of this profile is comprised of a secondary, steeply inclined reverse fault, with a fault plane attitude of 260°∠88°. Due to the high degree of weathering, this fault is categorized as a thrust fault, based on the fault gouge and the dislocation direction of the upper and lower plates. The Gonghe Formation's footwall was impacted by F6 and is clearly inclined and distorted. In this area, the strata's dip angle steadily decreases eastward from F6 to F5 (Figure 4A). Specifically, the lower plate's attitude changes from 275°∠45° at F6, to 130°∠32° midway between F6 and F5, to 150°∠2° on the western side of F5 (Figure 4B). The F6 upper plate's attitude is indecipherable, due to landslide events and slope deposit cover. The most recent Dangjiasi thrust interface (F6-1) in the western part of the Chiqugou route section does

not outcrop, as it is buried under Late Pleistocene alluvial deposits.

In addition, geologic evidence reflecting the LongWuHe Formation's thrust over the Middle–Late Pleistocene Yellow River alluvial strata is observable in a gully west of Duolonggou village. On the northern bank of the South Yellow River, the Dangjiasi rock mass was thrusted onto the Gonghe Basin's Linxia Formation (Perrineau et al., 2011). This resulted in the Linxia Formation west of Waliguan Mountain standing 200 m higher than its counterpart in the eastern Qunaihai sub-sag.

As discussed before, the Middle–Late Pleistocene Yellow River alluvial gravel deposit is the youngest strata impacted by the Waliguan Mountain thrust nappe, which indicates that the thrust napping activity distinctly weakened during the middle of the Late Pleistocene. In the south, the activity is stronger and the duration is longer, as compared to the north. The northern section is dominated by thrusting with dextral strike-slip in the early stage, whereas the southern section depicts occasional dextral strike-slip activity with thrusting occurring during the Late epoch.

3.2 Strike-slip–thrust nappe structure and spatiotemporal evolution

AFT thermochronology is commonly used to determine the uplift history of shallow crustal mountains (5–8 km) (Sobel and Dumitru, 1997; George et al., 2001; Sobel et al., 2003; Zheng et al., 2003). Previous AFT thermochronological studies on bedrock from mountains throughout the Gonghe Basin suggest that Ela Mountain, which is located in the southwest, started to uplift and become rapidly exposed ~25 Ma (Lu et al., 2012). In contrast, the northern Qinghai Nanshan and the southern Guinan Nanshan began to rapidly uplift 11–9 Ma and 10–7 Ma, respectively (Craddock, 2011). AFT thermal chronology results from Dangjiasi rock mass samples show rapid uplift was initiated in this area ~8–5 Ma (unpublished data). On the west of Waliguan Mountain, the bottom of the Linxia Formation is bordered by a layer of granitic weathered sands with basal conglomerate features. This stratum forms an angular unconformity west of the Dangjiasi rock mass. This phenomenon indicates that Waliguan Mountain was swiftly elevated and thrusted to the NE during deposition of the Linxia Formation.

The front margin of the strike-slip–thrust nappe structure belt at Waliguan Mountain consists of three imbricate strike-slip–thrust faults. From east to west, these include the Duolonggou Arc Fault (F4), Shangjiangou Fault (F6), and Waliguan Fault (F7). These faults, in combination with three additional NE-dipping faults on the west slope—F8, F9, and F10—constitute Waliguan Mountain's thrust nappe system, which depicts a positive flower structure. Waliguan Mountain has a large-scale thrust structure that is influenced by the boundary faults on the east and west sides.

Considering the north–south direction, there are significantly more branch faults in the south, as F4 and F6 primarily confine the branch faults in the north. The LongWuHe Formation and Dangjiasi rock mass comprise this nappe, while Late Pleistocene–Holocene alluvial fans cover the majority of the lower plate. To date, the most recent stratum impacted by the branch faults in the north remains undetermined. Oblique scratches are occasionally found in the fracture zone, which is thought to have been active throughout the Pliocene. These branch faults are primarily distinguished by the presence of thrust nappes. Contrarily, the southern part of Waliguan Mountain's thrust nappe belt is characterized by multibranch faults comprised of fault bundles—such as F4, F5, and F6. There are numerous oblique scratches in the Dangjiasi rock mass fracture zone, which suggests dextral strike-slip behavior. The F5 sliced through the Gonghe Formation. Ancient Yellow River alluvial deposits are the most recent stratum impacted by the footwall. These observations suggest that the southern section of the nappe, which became active in the Early Pleistocene to Middle–Late Pleistocene, is characterized primarily with dextral strike-slip movement accompanied by a thrust nappe from west to east.

The previously described phenomena demonstrates that as the thrust nappe and dextral strike-slip movements developed, the northwest section of this nappe continued to compress and shift northeastward in response to the clockwise rotation around Waliguan Mountain's vertical axis. In addition, the front fault's strike gradually shifted from NW to NNW, while the fracture zone was simultaneously narrowed. The most recent stratum impacted by this tectonic activity was continually buried beneath the footwall. In contrast, thrust nappe activity in the southern part of the nappe continued to develop with a backward expansion from east to west. Although the fracture zone for a single fault is narrower in the south than in the north, the southern area has more branch faults and oblique scratches within the Gonghe Formation. These observations suggest that Waliguan Mountain thrust nappe was dominated by thrust napping and dextral strike-slip movement during the Pliocene and primarily dextral strike-slip movement from the Early Pleistocene to the middle stage of the Late Pleistocene.

3.3 Analyzing the direction of maximum principal tectonic stress based on the strike-slip–thrust nappe structure

3.3.1 Depicting the direction of maximum principal tectonic stress based on the archery principle

When determining the direction of maximum principal tectonic stress (σ_1), the thrust nappe can be considered a structural style created by an extrusion system comprised of imbricate thrust faults. The imbricate thrust faults are a common

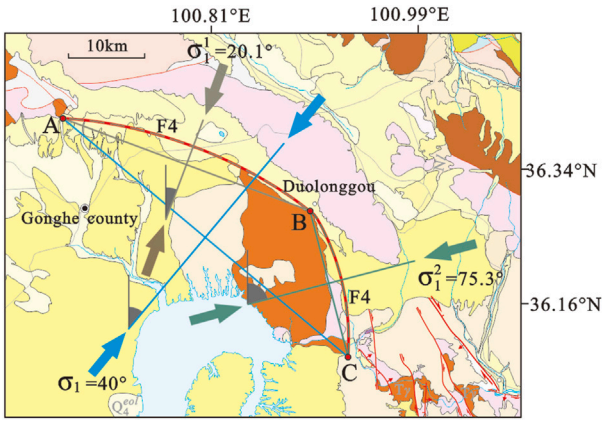

FIGURE 5
Determination of maximum principal tectonic stress (σ1) based on the Archery principle.

fault combination produced under a primarily horizontal tectonic stress field (Li et al., 2017). The tectonic extrusion direction is perpendicular to the strike of the leading-edge fault, namely the macroscopic tectonic direction. Therefore, the arching concept can be utilized to determine the maximum tectonic stress direction (σ_1). Applying the arching concept to the bow-shaped fault within the Duolonggou arc fault, the bow-shaped fault's two extremities were connected with a string. Subsequently, a vertical line was drawn from the string's midpoint to the top of the arc. This line represents the direction of maximum principal tectonic stress (σ1). The directions of minimum (σ3) and middle principal tectonic stress (σ2) are parallel and perpendicular to the string, respectively.

For diagramming purposes, the figure is split into AB, BC, and AC arcs based on the different distinguishing features between the northern and southern arcs in Duolonggou village. The top arcs AB, BC, and AC indicate the direction of maximum principal tectonic stress (σ1 1) during the early-stage thrust nappe, the maximum principal tectonic stress (σ2 1) during the late-stage thrust nappe, and the intermediate value of the maximum principal tectonic stresses (σ_1) during the early and late stages, respectively. The results from this study show that σ1 1, σ2 1, and σ1 in the study area equal 20.1°, 75.3°, and 40.0°, respectively (Figure 5).

The intermediate value (σ1) obtained before approximates that of the nearest Longyangxia dam area (Ma and Qi, 1993) and the Laxiwa hydropower station (Dong and Chen, 2003), indicating that this method is suitable for analyzing the Late Cenozoic tectonic stress field in the Qiabuqia area.

3.3.2 Tectonic stress field determination based on the fault's slickenside

Systematic sampling of obvious fault slickensides throughout the structural profile on the eastern foot of the Waliguan relay station indicated that the fault planes that formed during the early stage dipped to the SW at a 35° angle. Furthermore, well-developed slickensides and lineations showed that thrusting occurred in the NE direction (Figure 3A). Early-stage NW-trending thrust faults are crosscut by later-stage strike-slip faults that are striking SN and dipping at ~60°. Slickensides and lineations on the fault planes show dextral strike-slip activity (Figure 3D).

To obtain the triaxial stress orientation, STEREO.EXE software (Table 1) was used to reflect the tectonic stress field for a dextral oblique fault that lies within the southern Duolonggou arc fault and is characterized by clear slickensides. The results show that the σ1, σ2, and σ3 attitudes are 214.0°∠2.5°, 349.9°∠86.5°, and 108.7°∠1.7°, respectively. In summary, the stress associated with σ1, which strikes from 34°–214°, is nearly horizontal.

4 Geological characteristics of normal faults

In the study area, normal faults with small fault displacement are primarily found in the Linxia Formation (N_2l), Gonghe Formation ($Q_{1-2}^{al-l}g$), Middle–Late Pleistocene Yellow River alluvial strata (Q_{2-3}^{al}), and the Middle–Late Pleistocene alluvial–diluvial–swamp accumulation layers (Q_3^{2apl-l}) (Figure 6). However, these faults were all observed at outcrop scales and do not cut through modern slope alluvium. Consequently, the surface fault traces are difficult to recognize.

4.1 Geological features of the primary normal faults

4.1.1 Normal faults within the Linxia Formation

The stepped fault system west of Tulin (Fn1): Fn1 is in the Linxia Formation (N_2l), which is located east of the Qiabuqia Town–Longyangxia Highway and west of the Longyangxia Forest Geopark (Figure 7). The southern fault (Fa) has an attitude of 145°∠65°, and the grey-green mudstone marker bed is dislocated downward along the dip for 0.6 m. Similarly, the northern fault (Fb) has an attitude of 125°∠70°, with the grey-green mudstone marker bed dislocated downward along the dip for 0.55 m (Figures 7A,C). Oblique fault slickensides can be evident along the fault plane, suggesting that this fault is part of the normal–dextral strike-slip fault.

Using the third layer as the marker bed, the Fa fault offset measured 0.60 m. Joint fissures accompanied by the drag structure are prevalent around the fault, indicating that the fault be classified as normal. Using the second layer as the marker bed, the Fb fault offset measured 0.60 m (Figures 7C,D). In addition, joint fissures are commonly found to the south (Figure 7B), and the fault slickensides demonstrate dextral oblique thrust.

TABLE 1 Results of the tectonic stress field reflection using fault slickensides in the southern Duolonggou Arc Fault.

Postion	Number of the outcrop	Number of scratches/band	σ_1		σ_2		σ_3	
			Dip/°	Dip direction/°	Dip/°	Dip direction/°	Dip/°	Dip direction/°
Duolonggou	S717	8	220.9	11.2	316.3	25.3	89.0	55.1
	S718	8	34.6	16.1	142.8	47.3	275.2	31.9
	S722	5	248.0	1.7	342.5	70.0	165.9	19.9
	S724	8	183.4	15.1	261.5	62.9	274.6	23.2
Waliguan Moutain	S717	29	214.0	2.5	249.9	86.5	108.7	1.7
	S718							
	S722							
	S724							

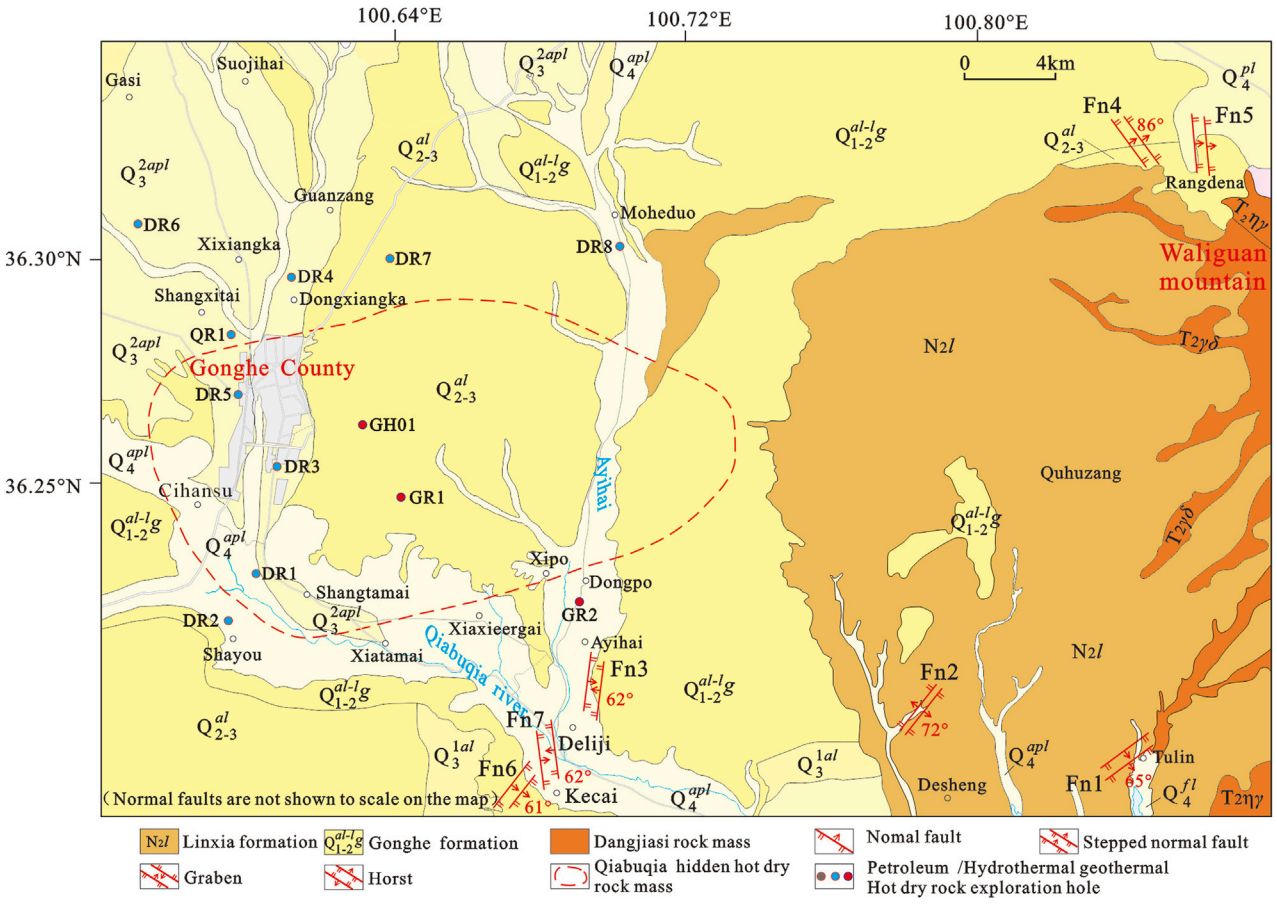

FIGURE 6
Distribution of normal faults in the Qiabuqia area (Area B in Figure 1B).

4.1.2 Normal faults in the Gonghe Formation (Fn2)

Normal faults in the Gonghe Formation are dominated by a graben-type structural framework. In the north central part of Ayihai gully, five typical faults with opposite dips were observed in the mudstone section of the Gonghe Formation. From northwest to southeast, the faults have attitudes of 295°∠75°, 300°∠70°, 305°∠70°, 125°∠60°, and 140.0°∠70°, and the associated

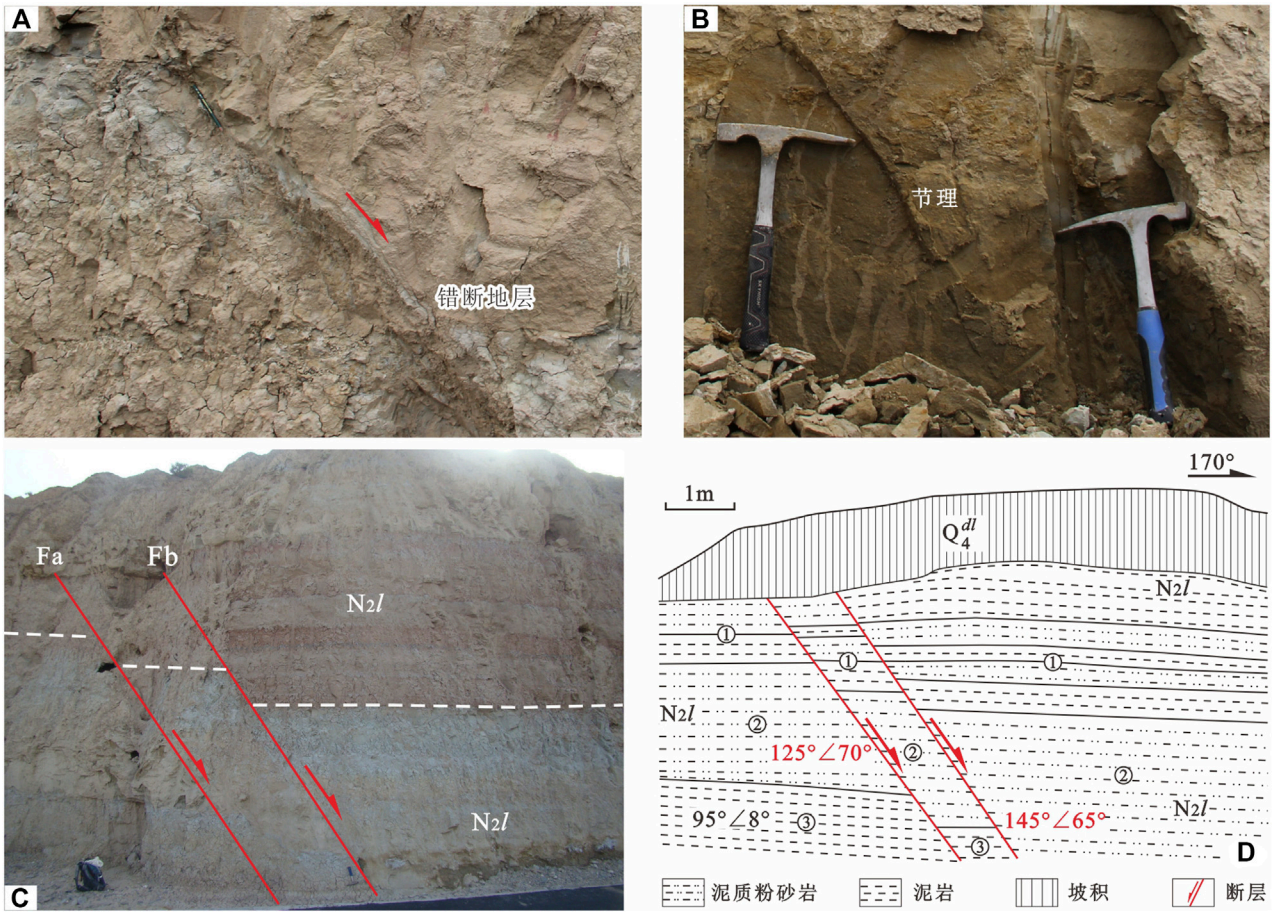

FIGURE 7
Step fault system west of Tulin (Fn1).

strata's attitudes range from 280°∠15° to 310°∠18°. Due to the absence of unique maker beds, the fault displacements were not measurable. However, the presence of vertical down-slip slickensides on the fault planes suggests that they are normal faults (Figures 8A,B).

The T1 terrace, which is located in the middle of Ayihai gully, is characterized by an evident ~0.05 m wide fault gouge and a secondary gypsum layer depicting S-shaped deformation (Figures 8C,D). The attitudes of the fault plane and associated stratum are 320°∠72° and 340.0°∠18°, respectively. The presence of clear downward-gliding slickensides on the fault plane suggests it's a normal fault.

In the Gonghe Formation located in the north central part of Ayihai gully, four normal faults with opposite dips were discovered under modern riverbed gravel deposits. From west to east, these faults have attitudes of 272°∠65°, 110°∠60°, 140.0°∠58°, and 295°∠72°, respectively (Figure 8C). The attitude of the associated stratum is 250°∠20°. The horizontal distance between adjacent faults from west to east is ~7, 3, and 10 m, respectively. The conglomerate marker bed successively dislocated downward along the dip for 0.50, 0.80, 0.05, and 1.0 m, respectively. The vertical downward-slipping slickensides on the fault planes demonstrate that they are also normal faults.

Similar graben structures that extend nearly south to north are common throughout many localities in north Deliji Village at the gully entry to Ayihai Valley (Figure 8F). The grabens are made up of two or more normal faults (Fn2) with the same characteristics; that is, they strike nearly parallel but dip in opposite directions. In profiles A and B, which span north–south, the Fa and Fb normal faults control the same graben structure (Figures 9A,B). The Fa fault has an attitude ranging from 97°∠58° to 101°∠62°, whereas the Fb fault's attitude is 283°∠62°. In profile A, the two faults are 3.10 m apart, yet in profile B the separation increased to 8.5 m.

As shown in profile B, the strata on both sides of the Fa fault are clearly dislocated, and the echelon shear joints are well developed (Figures 9C,D). These characteristics are typical of

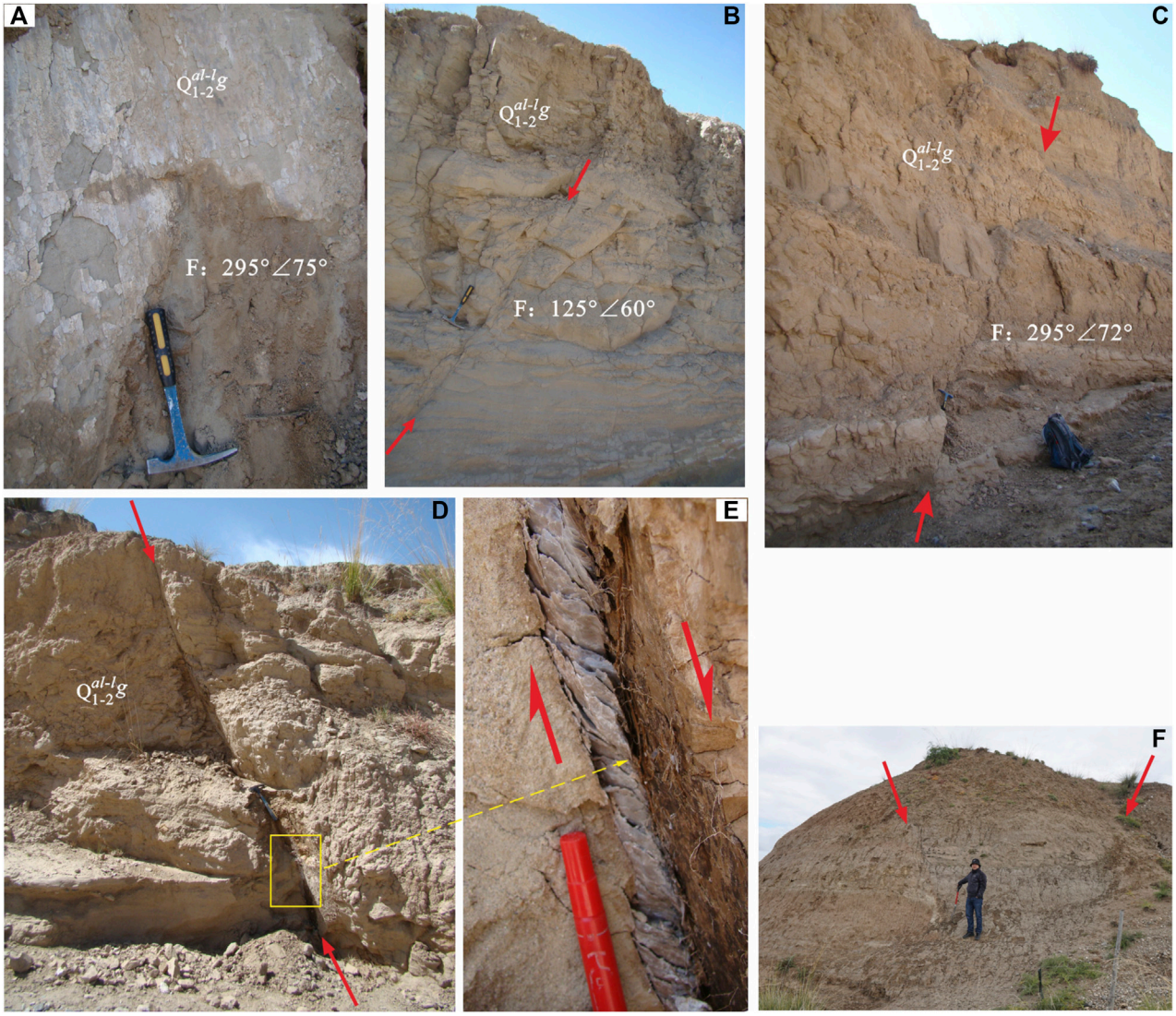

FIGURE 8
NS-trending normal faults along Ayihai gully. **(A,B)** Normal faults in northern Ayihai Valley. **(C,D,E)** Normal faults and S-shaped shear joints in central Ayihai Valley. **(F)** Combination of graben normal faults north of Dejilicun in southern Ayihai Valley.

normal faults. In profile A, the strata in the upper and lower plate of the Fa fault are also obviously dislocated and somewhat dragged (Figure 9E); features that are also commonly associated with normal faults. The Fb fault in profile A cuts across the Gonghe Formation strata. On both sides of the fault, the strata have distinct coloring and lithologies. From the bottom up, the upper plate is characterized with brown-red-yellowish silty mudstone, brown-red mudstone with grey-green mudstone, grey-green sandy mudstone, and grey-white sandy mudstone. The footwall consists of maroon mudstone, green fine siltstone, and grayish-yellow medium fine sandstone (Figures 9F,G). The strata's drag phenomena is indicative of the normal fault's behavior. While both the Fa and Fb faults lack comparable marker beds, it is assumed that these two faults have relatively large displacements.

4.1.3 Normal faults within the Middle–Late Pleistocene Yellow River alluvial strata

(1) Stepped normal fault system west of the Randena sand mining field (Fn3):

Two normal faults separated by 2–3 m were observed in an artificial profile of the Middle–Late Pleistocene Yellow River alluvial layer (Figures 10E,F). These faults do not cut through the overlying modern humus layer. The eastern fault consists of two wedge-shaped secondary faults that dip in opposite

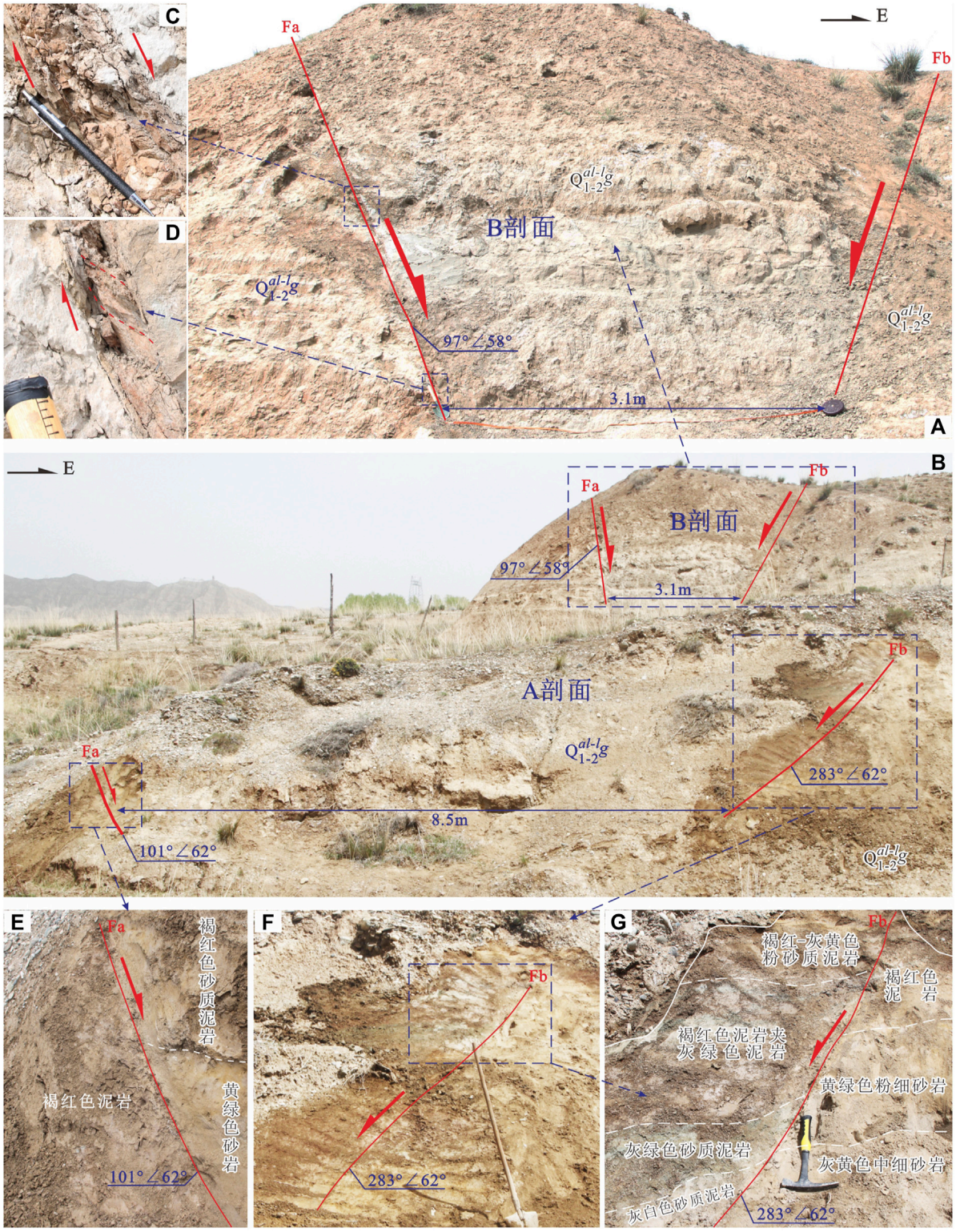

FIGURE 9
Graben-type normal fault framework north of Deliji village (Fn2).

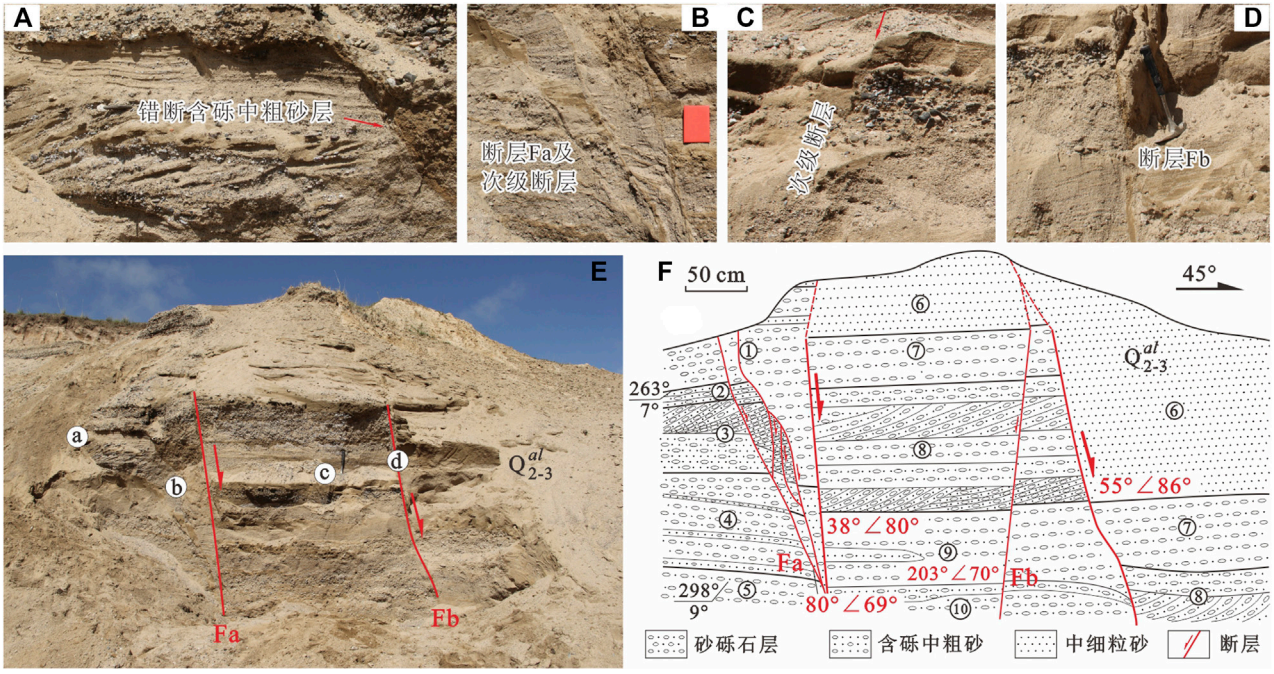

FIGURE 10
Stepped normal fault system west of the Rangdena sand mining field (Fn3).

directions. The fault's attitude is 55°∠86°, and the fault zone is 0.01–0.02 m wide and filled with sand. The marker bed in the upper plate moved downward more than 1.50 m. The western fault has an attitude of 203°∠70°, and is characterized with a 0.01–0.02 m wide fault zone. The marker bed on the upper plate dislocated downward ~0.05–0.10 m.

The western fault is composed of three secondary faults. Among them, the eastern and western branch faults have attitudes of 38°∠80° and 30°∠69°, respectively. The eastern branch fault has a 0.01–0.02 m wide fault zone that is filled with sands. Moreover, the marker bed in the upper plate is estimated to have moved downward for more than 1.50 m. Similarly, there is also a 0.01–0.02 m wide fault zone, with the marker bed of the upper plate being moved downward for about 0.05–0.10 m. A 0.05–0.20 m wide crumpled band developed in the sliding blocks that are controlled by the western, eastern, and middle branch faults. Here, the marker bed moved downward ~0.11 m. From SW to NE, the fault structures in the sedimentary layer have the following characteristics:

The Fa fault, is characterized by a 0.05–0.07 m wide disturbance zone and a fault plane attitude of 38°∠80°. The fault displacement is inferred to be >1.90 m, based on the corresponding relationships of the sedimentary assemblages. Four sets of secondary normal faults are on the west side of the fault; the lower ends of which intersect with the primary F1 fault. The marker beds are defined by medium-coarse pebbled sand and medium-coarse gravel sand with horizontal and oblique bedding (Figures 10C,D). From SW to NE, the fault displacements are 0.08, 0.04, 0.020, and 0.17 m, respectively. The Fb fault is characterized by 0.07–0.08 m wide fault gouges/sands and a fault plane attitude of 55°∠86°. Sand, gravels, and medium-coarse grained pebbled sand layers with oblique bedding served as marker beds and suggest a fault distance of ~1.50 m (Figure 10A). Between the principal Fa and Fb faults is a minor secondary normal fault with a fault plane attitude of 203°∠70° and a fault displacement of 0.055 m. Given the attitude of this secondary fault, it cut across different sedimentary layers (Figure 10B).

(2) Stepped normal fault system north of the Rangdena sand mining field (Fn4):

Fn4 consists of two normal faults separated by 0.60–1.20 m. The eastern fault has an attitude of ~82°∠45° and does not cut through the ~1.00 m thick alluvial gravel deposit at the top. In addition, the hanging wall's conglomerate marker bed moved upward ~0.05 m. Similarly, the western fault has an attitude of 70°∠68°, and also does not cut through the ~0.6 m thick alluvial gravel deposit at the top. In this case, the conglomerate marker bed on the hanging wall moved downward ~0.58 m. There is no evidence that the fault may extend deeper into Earth's interior.

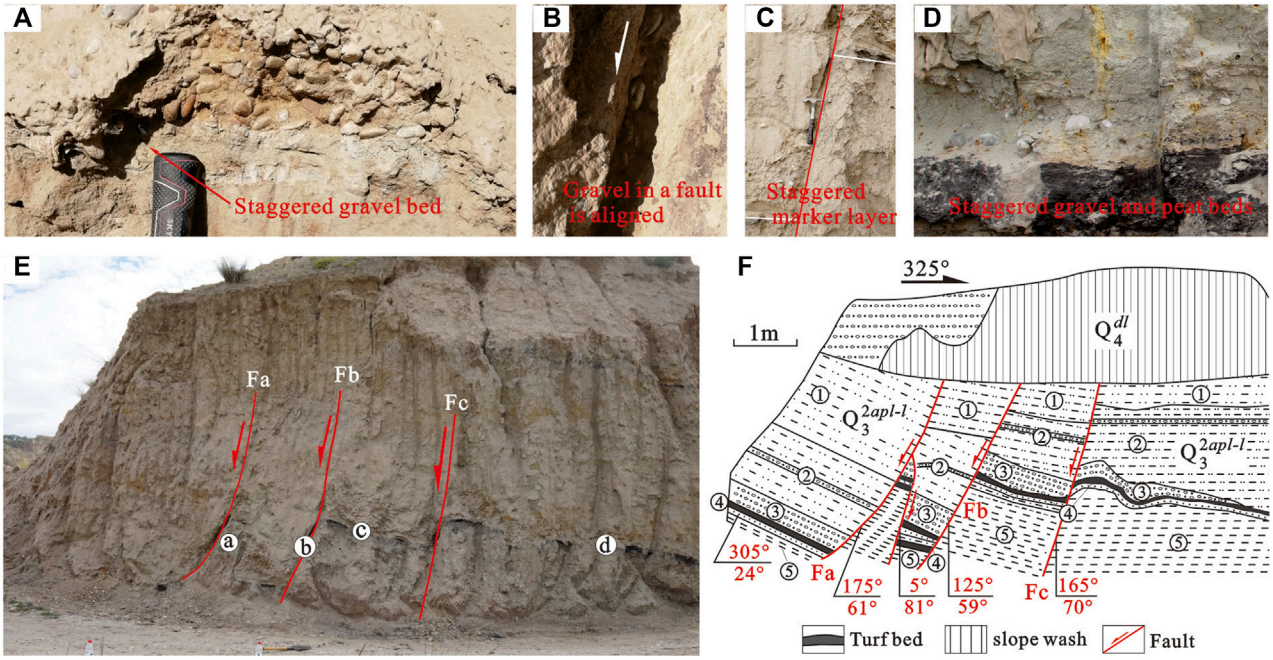

FIGURE 11
Stepped normal fault system in northwestern Kecai village (Fn5).

4.1.4 Normal faults in alluvial–flood strata intercalated with marsh strata during the Middle to Late Pleistocene

Stepped normal fault system northwest of Kecai Village (Fn5): The Fn5 profile is located northwest of Kecai Village, in front of a high terrace on the west side of the Qiabuqia River. Along the artificial cutting slope north of the makeshift road is a ~10 m long and 4.50 m high exposed profile composed of Late Pleistocene alluvial–flood accumulation strata intercalated with the marsh accumulation strata (Q_3^{2apl-l}). Two sets of normal faults were observed in the Late Pleistocene conglomerate/peat interlayers. One of those sets is characterized by an overall NE-NNE strike and SE dip, and consists of 3–4 secondary faults (Figures 11E,F). The other set generally strikes NE and dips SE, and is comprised of 3–4 secondary faults with attitudes of 135°∠40.0°, 128°∠58°, and 170°∠55°, respectively. The conglomerate marker beds are dislocated downward by 0.70, 0.95, and 0.50 m, respectively, demonstrating that it is a normal fault.

The Fa fault clearly cuts through the sand gravel, argillaceous silt, and peat layers. Along the fault fracture zone, the sand gravel shows directional alignment with the flat horizontal surface, and thus, is parallel to the fault plane, which has an attitude of 175°∠61° (Figure 11A). Using the gravel layer as the marker bed, the measured fault displacement is 0.93 m. A small secondary fault that cuts through the sand gravel, argillaceous silt, and peat layers is visible north of the Fa fault. The sand gravel along this fault fracture zone is also oriented with the flat horizontal surface and therefore is parallel to the fault plane, which has an attitude of 5°∠81°. Again, using the gravel layer as the marker bed, the measured fault displacement on this secondary fault is 0.60 m.

The Fb cuts across the sand gravel and peat strata. As observed in the Fa fault, the gravel shows directional alignment with the flat horizontal surface, and thus, is parallel to the fault plane, which has an attitude of 125°∠59° (Figure 11B). Using the gravel layer as a marker bed, the measured fault displacement is 1.15 m.

The Fc has a fault plane attitude of 165°∠75° and is comprised of gravel layers (Figure 11C). The measured fault displacement is 0.40 m. A secondary fault on the north section of Fc clearly dislocated the gravel and peat layers (Figure 11D).

4.2 Analysis of a normal fault's tectonic environment and formation time

Normal faults can be formed in multiple tectonic environments due to a myriad of geologic processes. Specifically, these include: 1) passive continental margin and rifting extensional environments (Qian, 1994); 2) fault bending in strike-slip fault systems and lateral jointing in local extensional environments (Woodcock and Fischer, 1986); 3) wedge extrusion structures or tunnel flows (Yin, 2006; Wang et al., 2016); 4)

refolding of thrust folds (fake 'normal fault') (Boyer and Elliott, 1982; Xiao et al., 2013; Thornton et al., 2018); 5) macroscopic anticline neutral outer arc extensional environments (Ramsay and Huber, 1987); and 6) alternating pressure–tension environments. In the latter case, once a symbiotic nappe and slippery nappe undergoing deformation show extrusion features, the "pushing first and sliding then" mechanism is initiated and relaxation/extension cyclicity occurs. As a result, during later extension, the thrust fault created during the extrusion deformation period develops such that the dip slip is opposite to the thrust direction. During this time, new normal faults may develop. Furthermore, as the temperature rises in the deep crust, the stress field undergoes horizontal tension in the upper crust and horizontal compression in the deeper crust. Tensile and compressive stresses are proportional to temperature gradients. This type of tensile stress can result in the formation of tensile structures. The surface tensile stress is greatest above the temperature-increasing zone, while the tension rapidly decreases on both sides and changes to compressive stress (Wang et al., 1999). Therefore, typical normal faults can form in a variety of situations. As such, because normal faults form in so many varied environments, and they cannot be exclusively used to decipher the geologic history.

In the Qiabuqia region, normal faults with a small degree of displacement generally show a similar set of characteristics. Specifically, normal faults with dispersed development positions are mostly found in sedimentary layers within the Linxia Formation and in Middle–Late Pleistocene period layers between Qiabuqia Town and Waliguan Mountain. Surface observations show that these normal faults have extremely short extensional lengths along the strike and small fault displacements along the dip, indicating that they are quite minor. Stepped and horst to graben structures are all observed in typical fault systems, while the profile structures are distinct and unrelated to one another. NE–SW, NW–SE, and near E–W strikes are all visible in the field outcrops. These fault planes show the distribution directions that are incompatible with one another, and they differ from the representative radial or zonal normal fault systems generated by the deep thermal dome structure (Liu, 2010). According to the statistical analysis results, only the graben-type normal fault systems that depict a roughly S-N extension in the Kecai–Deliji villages–Ayihai region extend relatively further. However, the scale and formation time of these normal faults' is significantly smaller than those of the graben system in the southern Qinghai–Tibetan Plateau, and thus are not regional. Regional geological surveys have shown that normal faults in the Gonghe Basin are mostly concentrated in the vicinity of Qiabuqia Town, west of Waliguan Mountain. Moreover, the deep basement structure demonstrates the presence of a relatively stable west-dipping slope belt. The possibility that this area was influenced by a nearly south–north extrusion associated with the Qinghai's southern mountain cannot not be excluded. The consistency of the tectonic stress system that caused the normal faults to develop in the Qiabuqia region remains unknown.

Based on the results presented before, this study divides the short displacement normal faults in the Qiabuqia region into two potential categories: 1) The Kecai village–Ayihaigou fault, which is associated with the Fn3 and Fn7 graben-type normal faults. This association came about due to the "brake" effect following the intense thrust nappe–dextral strike-slip activities of the Waliguan Mountain thrust nappe during the Middle–Late Pleistocene period. This "brake" effect caused the Qiabuqia region's shallow section on the trailing edge to relax and extend, resulting in the development of these new normal faults. 2) The Fn4 and Fn5 faults in the Rangdena area, northwest of Waliguan Mountain; and the Fn1 and Fn2 faults in the Tulin–Desheng village area, southwest of Waliguan Mountain. These associations were generated during the clockwise rotation around the vertical axis of the late Waliguan Mountain thrust nappe's right lateral strike slip. Under the tensional tectonic environment in the northwest and compressional tectonic environment in the southwest, the result is comparable to the pressure shadow trailed on both ends of the rotational speckles.

4.3 Direction of maximum principal tectonic stress analysis based on normal fault structural interpretation

4.3.1 Analyzing the direction of maximum principal tectonic stress based on the Anderson fault model

When using the Anderson fault model (Craddock et al., 2014) to analyze the stress state of a fault, it is generally believed that the fault plane of a brittle fault, on (near to) the surface, is a shear fracture plane. Thus, the σ_1 and σ_3 directions are consistent with acute and obtuse angle bisectors between two shear fracture planes. The plate where σ_1 is located will slide to the acute angular point, meaning the fault's upper and lower plates slide perpendicular to the σ_2 direction. The stress states of a normal fault consist of: maximum principal stress (σ_1), which is vertical; intermediate (σ_2) and minimum (σ_3) principal stresses, which are horizontal, while the σ_2 direction is consistent with the fault's strike. A Mohr's circle diagram depicting the stress states associated with normal fault formation shows that horizontal stretching and vertical uplifting are the most suitable stress states to form a normal fault. Under these circumstances, the maximum (σ_1) or minimum (σ_3) principal stresses gradually increase vertically or decrease horizontally. Therefore, according to the Anderson fault model, the σ_1, σ_2, and σ_3 directions in the Qiabuqia area are perpendicular, consistent, and horizontal, respectively, to the normal fault's strike.

TABLE 2 Tectonic stress field results for normal faults in the Qiabuqia area, as reflected by slickensides.

Outcrop location	Number of the outcrop	Number of slickensides/band	σ_1		σ_2		σ_3	
			Dip/°	Dip direction/°	Dip/°	Dip direction/°	Dip/°	Dip direction/°
Ayihai gully	S705	10	106.4	82.6	212.2	2.0	302.6	10.8
	S706	5	179.7	81.3	44.3	6.2	313.9	3.6
	S707	5	30.1	86.9	223.5	3.1	133.3	4.6
	S708	5	151.8	80.6	51.5	1.7	321.1	11.5
	S709	8	38.0	82.3	199.8	7.3	290.4	4.8
	S710	5	73.1	81.1	214.4	6.9	305.5	9.0
	S705–S710	38	98.0	85.4	215.9	2.2	306.2	6.2
Upper Qiabuqia River	S711	8	118.4	77.4	210.3	0.4	300.3	10.3
Data merging	S701–S711	46	106.3	83.9	214.6	1.9	304.8	7.2

4.3.2 Reflecting the maximum principal tectonic stress direction based on the normal fault slickensides

In this case, STEREO.EXE software was used to reflect the tectonic stress field's (σ1, σ2, and σ3) triaxial stress orientations of 46 sets of slickenside data obtained from normal faults in the Qiabuqia area (Table 2). The results show that the attitudes of σ_1, σ_2, and σ_3 are 106.3°∠83.9°, 214.6°∠1.9°, and 304.8°∠7.2°, respectively. The σ_1 direction is nearly vertical, whereas the σ_2 and σ_3 directions are both nearly horizontal. The fault's strike varies from 34.6° to 214.6°, while the direction of minimum principal stress, that is, the tensile stress, ranges from 124.8° to 304.8°.

5 Inference of the deep fault structure and analysis of the tectonic stress field

5.1 Inference of the deep basement fault structure in the Qiabuqia area

Although there is a NNW–SN-trending fault in the northern Nanshan–Gouhou Reservoir near Qiabuqia Town, it is cut off by a nearly E–W trending fault on the southern margin of Nanshan Mountain. This latter fault underwent dextral strike-slip during the Late Triassic–Cretaceous and has undergone left-lateral strike slip since the Paleogene. Therefore, the comparable southern *in situ* fault system is less likely to extend deep into the Qiabuqia area. As a result, the deep fault structure in the Qiabuqia region is related to the fault structure formed east of Waliguan Mountain.

The Riedel shear model (Figure 12) recognized four sets of faults in the Waliguan Mountain region (Figure 2), including the Duolonggou arc-shaped fault (F4) in the main displacement zone (PZD), four NW–NNW trending compression–torsion faults

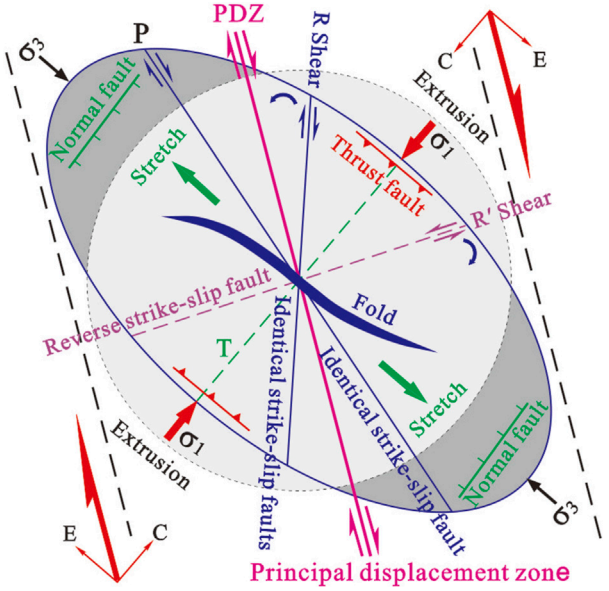

FIGURE 12
Illustration of the Riedel shear mode of the right strike-slip fault (Harding, 1974). *C, compression vector; E, extension vector; R, Riedel shear or same-directional strike-slip fault; R′, conjugate Riedel shear or reverse strike-slip fault; P, same-directional shear or secondary same-direction fault; T, local extension with shear; σ_1, maximum principal stress with a N-E direction; σ_2, intermediate principal stress with a vertical direction; σ_3, minimum principal stress with a N-W direction

(F8–F11)—i.e., Riddell same-trending secondary faults (P), three NNE–NE-trending tension–torsion faults (F14–F16)—i.e., Riedel local tensional (T) rupture, and three NWW compression–torsion faults (F13–F14)—i.e., conjugate Riedel (R′) reverse strike-slip faults. The Qiabuqia region's deep section is thought to contain three sets of the primary hidden

fault structures: the NW–NNW compression–torsion faults, the NE compression–torsion faults, and the NWW compression–torsion faults.

5.2 Analysis of the relationship between the cover and the basement fault

Geophysical investigation showed that the contact interface between the Qiabuqia hidden granite and the top of the Triassic metamorphic basement has a gentle slope form and gradually inclines to the west. There is no large-scale structural activation or arch deformation of the basement >20 m in length. Normal faults in the granitic body are characterized with a NE-NNE strike and are common in the north and east, but less so in the south and west. In the top sedimentary cover, a limited number of normal faults formed in the hanging wall of the NE-NNE trending basement thrust fault showed a "Y" shape. These faults have a fault displacement of <20 m and are parallel to the underlying basement structure, with more in the higher portion and less in the lower. Most of them do not cut through the Xianshuihe Formation. In the shallow level above the Xianshuihe Formation, there are normal faults scattered in all directions. However, in the deep level below the Xianshuihe Formation, normal faults are rare and mainly in the NE-NNE direction.

According to the aforementioned analysis, the top interface of the Xianshuihe Formation, controlled by the representative DR4 hole, may be buried at a depth of ~1,000 m. The top part of the Xianshuihe Formation shows tectonic stress states associated with a normal fault (NF), whereas in the deep basement, the tectonic stress states associated with a reversal fault (TF) accompanied by strike-slip (SS) movement are dominant. The Xianshuihe Formation's top interface is analogous to the "neutral plane" that presents as "tension at the top and thrust and strike-slip in the bottom" (Figure 13). As a result, the NE–NNE trending normal fault formed inside Qiabuqia's hidden granite body due to a tensile–torsional structural plane that formed concurrently with the Riedel shear mode T rupture. However, the normal faults visible on the surface extend only to a limited depth and cannot be used as a basis for judging the deep tectonic stress field.

5.3 Tectonic evolution and stress variation during the Late Cenozoic

Under the influences of the Qinghai–Tibetan Plateau uplift and the accompanying eastward extrusion of its northeast margin, as well as the far-field effect of the Indo–Asian plate collision, the Late Cenozoic tectonic evolution and stress variation in the Qiabuqia area can be divided into the following three periods:

(1) Thrust nappe accompanied by dextral strike-slip movement during the Late Miocene to Late Pliocene:

The *in situ* "granite weathered sand" layer with the basal conglomerate features at the bottom of the Pliocene Linxia Formation shows that Waliguan Mountain thrusted over and uplifted out of the surface during this period, similar to a peninsula stretching southeastward. While the area northeast of Waliguan Mountain lacks sedimentary records, fluvial-lacustrine deposits belonging to the Linxia Formation can, for the most part, be found in the west, south, and southeast parts. The mountain's eastern border has continually risen, owing to the fast uplift of the thrust nappe along the Duolonggou arc-shaped fault. Simultaneously, NNE-trending tensile–torsional faults, that is, Riedel local tension (T) rupture, NW-trending compressive–torsion faults that is, Riedel secondary syn-trending faults (P), and NWW-trending compressive–torsion faults have been revived or regenerated. The (σ1 1) direction was NNE 20.1° during this period.

(2) Dextral strike-slip accompanied by thrust nappe movement during the Early Pleistocene to the Middle–Late Pleistocene period:

During this time, the extent of uplift in Waliguan Mountain, generated by the thrust, continually increased. The Gonghe Formation sedimentation was almost completely surrounding Waliguan Mountain. Meanwhile, the Linxia Formation on the west part of Waliguan Mountain rose, whereas the Linxia Formation on the east dropped ~200 m below the Gonghe Formation. This might have resulted in simultaneous uplift and emplacement of the Qiabuqia hidden hot dry rock mass. During the Late Pleistocene, from the early to middle period, the magnitude of the dextral strike-slip and the clockwise rotation around the vertical axis of Waliguan Mountain progressively increased. The NW portion of the Duolonggou arc fault compressed and contracted, while the south segment pushed and napped. Within the Gonghe Formation, at least three fault bundles extended southward. This tectonic activity also caused these strata to tilt and formed local dips up to 45°.

The growth layers within the Gonghe Formation suggest that the Early–Middle Pleistocene thrust nappe event had a pulse development pattern. The thrust nappe event has most recently influenced the Middle–Late Pleistocene alluvial deposit from the ancient Yellow River. It is believed that the thrust nappe activity began to decline around the Middle–Late Pleistocene. The maximum principal tectonic stress direction shifted from NNE 20.1° during the early period to SSE 75.3° during the late

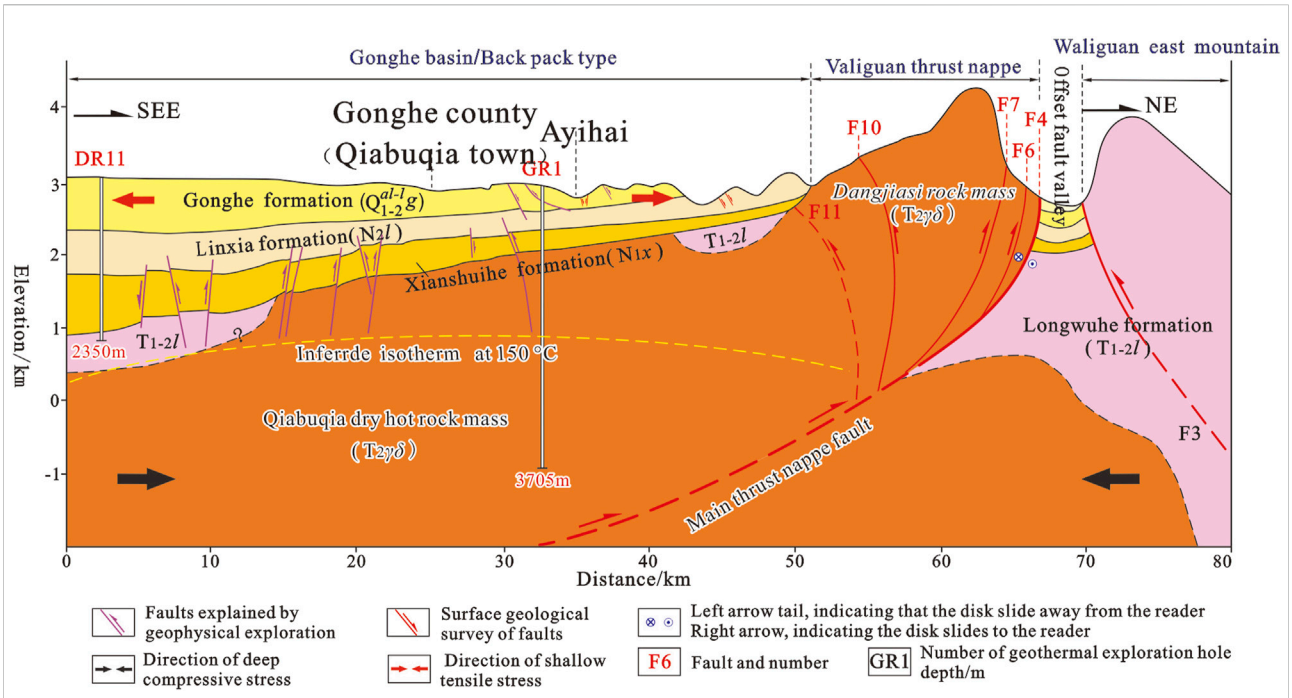

FIGURE 13
Structural profile of the Dalianhai–Waliguan and vertical structural changes of the tectonic stress field.

period, due to the Duolonggou arc fault's progressive transformation from thrust nappe to dextral strike-slip movement. Waliguan Mountain started to rotate clockwise along the vertical axis as the regional stress field shifted from NNE to SSE. Meanwhile, dextral strike-slip movement was introduced to regulate the eastward expansion of Waliguan Mountain. It may also have resulted in the formation of Fn4 and Fn5 in the Rangnade area, as well as Fn1 and Fn2 normal faults in the Tulin–Desheng Village area.

(3) Late Pleistocene to Middle Holocene—the "brake" period for the thrust nappe in Waliguan Mountain and relaxational extension for the shallow part of the trailing edge:

This geological body experienced a significant thrust nappe from the Early Pleistocene to the middle of the Late Pleistocene. However, the thrust nappe activity ceased in the Late Pleistocene, resulting in a "brake" effect for the trailing edge. Meanwhile, the surface of the western Qiabuqia region began to relax and stretch, forming a graben-type normal fault system with a roughly S–N trend in the Kecai–Deliji Village–Ayihai gully area.

In summary, using the buried depth of ~1,000 m at the top interface of the Xianshuihe Formation, the vertical structure of the tectonic stress field in the Qiabuqia area is a normal fault–type (NF) tectonic stress state for the upper part and a reverse fault–type (TF) plus strike-slip-type (SS) tectonic stress state for the lower part. The top interface of the Xianshuihe Formation is equivalent to a structural "neutral plane," depicting "tension at the upper part, but thrust and strike-slip at the lower part."

6 Conclusion

The following major conclusions can be drawn from the present study:

1. During the Late Cenozoic, the Qiabuqia region, which resides in the northeastern margin of the Gonghe Basin, experienced three stages of evolution: 1) thrust napping with occasional dextral strike-slipping during the Late Miocene–Late Pliocene; 2) occasional dextral strike-slipping with thrusting during the Early Pleistocene to Middle Pleistocene; and 3) "braking" of the thrust nappe in Waliguan Mountain, as well as relaxing and stretching of the shallow part in the trailing edge during the Late Pleistocene to Middle Holocene.
2. As demonstrated by the DR4 borehole, the Xianshuihe Formation is buried to a depth of ~1,000 m. The top part of this Formation is characterized by a normal fault–type (NF) tectonic stress state, whereas the reverse fault–type (TF) + strike-slip type (SS) tectonic stress state dominates in the deep basement. The upper normal fault's σ1 and σ3 are vertical and horizontal, respectively. As for the deep reverse fault + strike-slip, the σ1 is in the NE–SW direction and varies from 20.1° to 75.3°, yielding an average of 40.0°.

3. Based on the Riedel shear model, three types of hidden fault structures developed in the Qiabuqia region, that is, the NW–NNW trending compressional–torsional fault, the NE-trending tensional–torsional fault, as well as the NWW-trending compressional–torsional fault.

Data availability statement

The original contributions presented in the study are included in the article/Supplementary Material; further inquiries can be directed to the corresponding author.

Author contributions

ZY: The conception or design of the work, field investigation and analysis by synthesis, drafting and revising the work. Q: Field investigation, analysis by synthesis, map compilation and revising the work. FL: Analysis by synthesis, drafting and revising the work. ZC: Analysis by synthesis. ZL: Field investigation and analysis by synthesis. ZS: The conception or design of the work, field investigation and analysis by synthesis, map compilation. LD: Analysis by synthesis. YZ: Analysis by synthesis. SJ: Map compilation. FL: Analysis by synthesis. NZ: Field investigation.

Funding

This work was supported by the National Key Research and Development Program of China (No. 2018YFB1501801) and China Geological Survey Project (No. DD20190131).

Conflict of interest

The authors declare that the research was conducted in the absence of any commercial or financial relationships that could be construed as a potential conflict of interest.

Publisher's note

All claims expressed in this article are solely those of the authors and do not necessarily represent those of their affiliated organizations, or those of the publisher, the editors, and the reviewers. Any product that may be evaluated in this article, or claim that may be made by its manufacturer, is not guaranteed or endorsed by the publisher.

References

Anderson, E. M. (1951). The dynamics of faulting and dyke formation with application to Britain. *J. Geol.* 62 (4), 417. doi:10.1086/626182

Boyer, S. E., and Elliott, D. (1982). Thrust systems. *Am. Assoc. Petroleum Geol. Bull.* 66 (9), 1196–1230. doi:10.1306/03B5A77D-16D1-11D7-8645000102C1865D

Chang, H., Jin, Z. D., and An, Z. S. (2009). Sedimentary evidences of the uplift of the Qinghai Nanshan (the mountains south to Qinhai Lake) and its implication for tructural evolution of the Lake Qinghai-Gonghe basin. *Geol. Rev.* 55 (1), 49–57. (in Chinese with English abstract).

Chen, F. W., Wu, Z. Z., and Li, S. H. (2016). Three 1:50,000 regional geological and mineral survey reports of J47E022019, J47E022020, and J47E023020 in Dongba area, Gonghe County, Qinghai Province. Xining. Qinghai Provincial Department of Natural Resources Archives.

Christie-Blick, N., and Biddle, K. T. (1985). Deformation and basin formation along strike-slip faults. *Strike-Slip Deformation, Basin Form. Sediment.*, 1–34. doi:10.2110/pec.85.37.0001

Cowgill, E., Yin, A., Arrowsmith, R., Feng, W., and Shuanhong, Z. (2004). The akato tagh bend along the Altyn tagh fault, northwest tibet, 1: Smoothing by vertical-axis rotation and the effect of topographic stresses on bend-flanking faults. *Geol. Soc. Am. Bull.* 116, 1423–1442. doi:10.1130/b25359.1

Craddock, W. H., Eric, K., Huiping, Z., Marin, K. C., Jean-Daniel, C., and Daoyang, Y. (2014). Rates and style of cenozoic deformation around the Gonghe Basin, northeastern Tibetan plateau[J]. *Geosphere* 10 (6), 1255–1282. doi:10.1130/ges01024.1

Craddock, W. H., Kirby, E., and Zhang, H. (2011). Late Miocene-Pliocene range growth in the interior of the northeastern Tibetan Plateau[J]. *Lithosphere.* 3 (6), 420–438. doi:10.1130/l159.1

Craddock, W. H. (2011). *Structural and geomorphic evolution of the Gonghe basin complex, northeastern Tibet: Implications for the timing of plateau growth[D].* Pennsylvania, United States: The Pennsylvania State University.

Crowell, J. C. (1974). "Origin of late cenozoic basins of southern California,". Editor W. R. Dickinson (Oklahoma, United States: SPEM Special Publications), 22, 190–204. Tectonics and Sedimentation.

Deng, Q. D., Zhang, P. Z., Ran, Y. K., Yang, X. P., He, W., and Chu, Q. Z. (2002). Basic characteristic of active tectonics of China. *Sci. China (Ser D)* 32 (12), 1020–1030. (in Chinese with English abstract). doi:10.3321/j.issn:1006-9267.2002.12.007

Dong, L. F., and Chen, W. Y. (2003). Study on characteristics of *in-situ* stress field in laxiwa hydropower station. *Chin. J. Rock Mech. Eng.* 22 (S2), 2544. (in Chinese with English abstract). doi:10.3321/j.issn:1000-6915.2003.z2.002

Dooley, T., Mcclay, K., and Bonora, M. (1999). 4D evolution of segmented strike-slip fault systems: Applications to NW europe. *Geol. Soc. Lond. Pet. Geol. Conf. Ser.* 5, 215–225. doi:10.1144/0050215

Elliott, D. (1976). The energy balance and deformation mechanisms of thrust sheet. *Phil. Trans. R. Soc. Lond.* 238, 289–312. doi:10.1098/rsta.1976.0086

Fang, X. M., Song, C. H., Dai, S., Zhu, Y. T., Gao, J. P., and Zhang, W. L. (2007). Cenozoic deformation and uplift of the NE Qinghai-Tibet Plateau: Evidence from high-resolution magnetostratigraphy and basin evolution. *Earth Sci. Front.* 14 (1), 230–242. (in Chinese with English abstract). doi:10.3321/j.issn:1005-2321.2007.01.022

Fang, X. M., Yan, M. D., Voo, R. V. D., Rea, D. K., Song, C. H., Josep, M. P., et al. (2005). Late cenozoic deformation and uplift of the NE Tibetan plateau: Evidence from high-resolution magnetostratigraphy of the guide basin, Qinghai province, China. *Geol. Soc. Am. Bull.* 117 (9–10), 1208–1225. doi:10.1130/b25727.1

George, A. D., Marshalsea, S. J., Wyrwoll, K. H., Jie, C., and Yanchou, L. (2001). Miocene cooling in the northern Qilian Shan, northeastern margin of the Tibetan Plateau, revealed by apatite fission-track and vitrinite - reflectance analysis. *Geol.* 29 (10), 939–942. doi:10.1130/0091-7613(2001)029<0939:mcitnq>2.0.co;2

Harding, P. T. (1974). Petroleum traps associated with wrench faults. *AAPG Bull.* 58 (7), 1290–1304. doi:10.1306/83d91669-16c7-11d7-8645000102c1865d

Harding, T. P. (1985). Seismic characteristics and identification of negative flower structures, positive flower structures, and positive structural inversion. *AAPG Bull.* 69, 582–600. doi:10.1306/AD462538-16F7-11D7-8645000102C1865D

Jiang, R. B., Chen, X. H., Dang, Y. Q., Yin, A., Wang, L. Q., Jiang, W. M., et al. (2008). Apatite fission track evidence for two phases Mesozoic-Cenozoic thrust

faulting in eastern Qaidam Basin, 2008. *Chin. J. Geophys.* 51 (1), 116–124. (in Chinese with English abstract). doi:10.3321/j.issn:0001-5733.2008.01.015

Li, P., Su, S. R., Ma, C., Zhang, C. Y., and Chen, Y. H. (2017). Distribution law of crustal stress in different combina-tions of imbricate reverse faults. *J. Eng. Geol.* 25 (3), 637–647. (in Chinese with English abstract). doi:10.13544/j.cnki.jeg.2017.03.009

Li, Z. M., Tu, H. W., Tian, Q. J., Zhang, J. L., and Li, W. Q. (2010). The 2008 Ms 6.3 earthquake in the Dachaidan region, Qinghai Province and its seimotectonic setting. *Prog. Geophys.* 25 (3), 768–774. doi:10.3969/j.issn.1004-2903.2010.03.004

Liu, C. Y. (2010). Geologic and metallogenic or pool - forming effects of the thermodynamic process and their identification. *Oil Gas Geol.* 31 (6), 72. doi:10.11743/ogg20100605

Lowell, J. D. (1972). Spitsbergen tertiary orogenic belt and the spitsbergen fracture zone. *Geol. Soc. Am. Bull.* 83, 3091–3102. doi:10.1130/0016-7606(1972)83[3091:stobat]2.0.co;2

Lu, H. J., Wang, E. C., Shi, X. H., and Meng, K. (2012). Cenozoic tectonic evolution of the Elashan range and its surroundings, northern Tibetan Plateau as constrained by paleomagnetism and apatite fission track analyses. *Tectonophysics* 580, 150–161. doi:10.1016/j.tecto.2012.09.013

Luyendyk, B. P., Kammerling, M. J., and Terres, R. (1980). Geometrical model for Neogene crustal rotations in southern California. *Bull. Geol. Soc. Am.* 91, 211–217.

Ma, Q. C., and Qi, L. (1993). Three dimensional ground stress field and mechanism of fault zone at dam site of Longyangxia project. *Chin. J. Geotechnical Eng.* 15 (3), 1–8. (in Chinese with English abstract). doi:10.1007/BF02656947

Mann, P. (2007). *Global catalogue, classification and tectonic origins of restrainingand releasing bends on active and ancient strike-slip fault systems*, 290. London: Special Publications, 13–142. Geological Society.

McClay, K., and Bonory, M. (2001). Analog models of restraining stepovers in strike-slip fault systems. *AAPG Bull.* 85, 233–260. doi:10.1306/8626C7AD-173B-11D7-8645000102C1865D

Perrineau, A., Van Der Woerd, J., Gaudemer, Y., Jing, L. Z., Pik, R., Tapponnier, P., et al. (2011). Incision rate of the Yellow River in northeastern tibet constrained by 10Be and 26Al cosmogenic isotope dating of fluvial terraces: Implications for catchment evolution and plateau building. *Geol. Soc. Spec. Publ.* 353, 189–219. doi:10.1144/sp353.10

Qian, X. L. (1994). *Studies on extensional tectonics*. Beijing: Geological Publishing House, 166. (in Chinese with English abstract).

Ramsay, J. G., and Huber, M. I. (1987). *The techniques of modern structural geology: Volume 2 folds and fractures*. London: Academic Press, 309–700.

Sobel, E. R., and Dumitru, T. A. (1997). Thrusting and exhumation around the margins of the western Tarim Basin during the India-Asia collision. *J. Geophys. Res.* 102 (B3), 5043–5063. doi:10.1029/96jb03267

Sobel, E. R., Hilley, G. E., and Strecker, M. R. (2003). Formation of internally drained contractional basins by aridity-limited bedrock incision. *J. Geophys. Res.* 108 (B7), 2344. doi:10.1029/2002jb001883

Sun, Y. G., Fang, H. B., Zhang, K., Zhao, F. Y., and Liu, S. Y. (2007). Step-like landform system of the Gonghe Basin and the uplift of the Qinghai-Tibet Plateau and development of the Yellow River. *Geol. China* 34 (6), 1141–1147. (in Chinese with English abstract). doi:10.3969/j.issn.1000-3657.2007.06.021

Sylvester, A., and Smith, R. (1976). Tectonic transpression and basement controlled deformation in the San Andreas fault zone, Salton trough, California. *AAPG Bull.* 60, 2081–2102. doi:10.1306/C1EA3A73-16C9-11D7-8645000102C1865D

Thornton, J. M., Mariethoz, G., and Brunner, P. (2018). A 3D geological model of a structurally complex Alpine region as a basis for interdisciplinary research. *Sci. Data* 5, 180238. doi:10.1038/sdata.2018.238

Wang, J. M., Zhang, J. J., Liu, K., Zhang, B., Wang, X. X., Rai, S. M., et al. (2016). Spatial and temporal evolution of tectonometamorphic discontinuities in the central Himalaya: Constraints from P-T paths and geochronology. *Tectonophysics* 679, 41–60. doi:10.1016/j.tecto.2016.04.035

Wang, L. J., Ciu, J. W., and Wang, W. (1999). Tectonic deformation and thermal stress field in Qinghai - tibet plateau. *J. Geomechanics* 5 (3), 1–7. doi:10.3969/j.issn.1006-6616.1999.03.001

Wang, S. T., LiY, S., Su, D. G., and Wei, L. W. (1988). Engineering geological study of regional structural stability in the area of the Longyang Gorge hydro-electrical power station on the Huanghe (Yellow) river. *Acta Geol. Sin.* 62 (4), 361–372. (in Chinese with English abstract).

Wang, Z. C., Zhang, P. Z., Zhang, G. L., Li, C. Y., Zheng, D. W., and Yuan, D. Y. (2006). Tertiary tectonic activities of the north frontal fault zone of The west qinling mountains: Implications for the growth of the northeastern margin of the Qinghai-Tibetan plateau. *Earth Sci. Front.* 13 (4), 119–135. (in Chinese with English abstract). doi:10.3321/j.issn:1005-2321.2006.04.010

Westaway, R. (1995). Deformation around stepovers in strike-slip fault zones. *J. Struct. Geol.* 17, 831–846. doi:10.1016/0191-8141(94)00098-k

Woodcock, N., and Fischer, M. (1986). Strike-slip duplexes. *J. Struct. Geol.* 8, 725–735. doi:10.1016/0191-8141(86)90021-0

Wu, Y., Dai, J. S., Gu, Y. C., Shang, L., and Liu, Q. (2014). Numerical simulation of present geo-stress field and its effect on hydraulic fracturing of Fuyu reservoir in Gaotaizi oilfield. *J. Geomechanics* 20 (4), 363–371. (in Chinese with English abstract). doi:10.3969/j.issn.1006-6616.2014.04.004

Xiao, W., Windley, B. F., Allen, M. B., and Han, C. (2013). Paleozoic multiple accretionary and collisional tectonics of the Chinese Tianshan orogenic collage. *Gondwana Res.* 23 (4), 1316–1341. doi:10.1016/j.gr.2012.01.012

Xu, S. Y., Xu, D. F., and Shi, R. S. (1984). A discussion on the development of landforms and evolution of environments in the gonghe basin. *J. Lanzhou Univ.* 20 (1), 196–157. (in Chinese with English abstract).

Yang, L. Z., Sun, Z. X., Liu, J. H., Wang, A. D., and Wan, J. J. (2017). On deployment of high - temperature deep geothermal wells in typical areas with hot dry rock potential in China. *Geol. Explor.* 53 (2), 355–360. (in Chinese with English abstract). doi:10.12017/dzkx.2017.022

Yin, A. (2010). Cenozoic tectonic evolution of asia: A preliminary synthesis. *Tectonophysics* 488, 293–325. doi:10.1016/j.tecto.2009.06.002

Yin, A. (2006). Cenozoic tectonic evolution of the Himalayan orogen as constrained by along-strike variation of structural geometry, exhumation history, and foreland sedimentation. *Earth-Science Rev.* 76, 1–131. doi:10.1016/j.earscirev.2005.05.004

Yuan, D. Y., Zhang, P. Z., Liu, B. C., Gan, W. J., Mao, F. Y., Wang, Z. C., et al. (2004). Geometrical imagery and tectonic transformation of Late Quaternary active tectonics in northeastern margin of Qinghai-Xizang Plateau. *Acta Geol. Sin.* 78 (2), 270–278. (in Chinese with English abstract). doi:10.3321/j.issn:1005-2321.2004.04.006

Yuan, D. Y., Zhang, P. Z., Liu, X. L., Liu, B. C., Zheng, W. J., and He, W. G. (2004). The tectonic activity and deformation features during the Late Quaternary of Elashan Mountain active fault zone in Qinghai Province and its implication for the deformation of the northeastern margins of the Qinghai-Tibet Plateau. *Earth Sci. Front.* 11 (4), 393–402. (in Chinese with English abstract). doi:10.3321/j.issn:0001-5717.2004.02.017

Zeng, Z. P., Liu, Z., Ma, J., Zhang, C. L., Li, J., Liu, Z., et al. (2019). A new method for fracrability evaluation in deep and tight sandstone reservoirs. *J. Geomechanics* 25 (2), 223–232. (in Chinese with English abstract). doi:10.12090/j.issn.1006-6616.2019.25.02.021

Zhang, C. Y., Chen, Q. C., Qin, X. H., Hong, B., Meng, W., and Zhang, Q. F. (2017). *In-situ* stress and fracture characterization of a candidate repository for spent nuclear fuel in Gansu, northwestern China. *Eng. Geol.* 213, 218–229. doi:10.1016/j.enggeo.2017.10.007

Zhang, K., Liu, K., and Yang, J. (2004). Asymmetrical valleys created by the geomorphic response of rivers to strike-slip fault. *Quat. Res.* 62, 310–315. doi:10.1016/j.yqres.2004.07.003

Zhang, P. Z., Zheng, D. W., Yin, G. M., Yuan, D. Y., Zhang, G. L., Li, C. Y., et al. (2006). Discussion on Late Cenozoic growth and rise of northeastern margin of the Tibetan plateau. *Quat. Sci.* 26 (1), 5–13. (in Chinese with English abstract). doi:10.3321/j.issn:1001-7410.2006.01.002

Zhang, S. Q., Wu, H. D., Zhang, Y., Song, J., Zhang, L. Y., Xu, W. L., et al. (2020). Characteristics of regional and geothermal Geology of the reshuiquan HDR in guide county, Qinghai province. *Acta Geol. Sin.* 94 (5), 1591–1605. (in Chinese with English abstract).

Zhang, Y. Q., Liao, C. Z., Shi, W., and Hu, B. (2006). Neotectonic evolution of the peripheral zones of the Ordos basin and geodynamic setting. *Geol. J. China Univ.* 12 (3), 285–297. (in Chinese with English abstract). doi:10.3969/j.issn.1006-7493.2006.03.001

Zheng, D. W., Zhang, P. Z., Wan, J. L., Li, C. Y., and Cao, J. X. (2003). Late cenozoic deformation subsequence in northeastern margin of tibet: Detrital AFT records from Linxia basin. *Sci. China (Series D)* 33, 190–198. (in Chinese with English abstract). doi:10.3321/j.issn:1006-9267.2003.z1.021